Supporting Information for Direct Intramolecular Carbon(sp^2)-Nitrogen(sp^2) Reductive elimination from Gold(III)

Jong Hyun Kim[a], R. Tyler Mertens[a], Amal Agarwal[a], Sean Parkin[a], Gilles Berger[b], and Samuel G. Awuah[a]*

[a] *Department of Chemistry, University of Kentucky, 505 Rose Street, Lexington, Kentucky 40506, United States*
[b] *Microbiology, Bioorganic & Macromolecular Chemistry, Faculty of Pharmacy, Université Libre de Bruxelles, Belgium*

*awuah@uky.edu

TABLE OF CONTENTS

Supplemental materials and methods

Experimental Details

X-ray Crystallography. Crystal for **3** were grown at room temperature from a DCM reaction solution. Suitable crystals were selected by microscopic examination through crossed polarizers, mounted on a fine glass fiber in polyisobutane oil, and cooled to 90 K under a stream of nitrogen. A Bruker-AXS D8 Venture dual microsource diffractometer was used to collect the diffraction data using Mo$K\alpha$ radiation ($\lambda = 0.71073$ Å) from the crystal. The raw data were integrated, scaled, merged, and corrected for Lorentz-polarization effects using the APEX3 package[1]. Absorption correction was performed by SADABS[2-3] within APEX3. Space group determination and structure solution were carried out with SHELXT, and refinement used SHELXL-2017[4-5]. All non-hydrogen atoms were refined with anisotropic displacement parameters. Hydrogen atoms were placed at calculated positions and refined using a riding model with their isotropic displacement parameters (U_{iso}) derived from the atom to which they were attached. The structures, deposited in the Cambridge Structural Database, were checked with an R-tensor[6], by PLATON[7], and were further validated using CheckCIF[7]. See Figure S31and Table S1-S4 for structure details.

***N,N'*-(1,2-Ethanediylidene)bis-2,4,6-trimethylphenylamine**

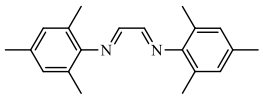

This procedure was modified from a previously modified.[8] A round-bottom flask was charged with 75 mL of methanol and 2,4,6-trimethylaniline (20.63 mL, 15 mmol). The mixture was stirred until all the primary amine had dissolved. To this solution, glyoxal (40% aqueous solution, 3.40 mL, 70 mmol) and a catalytic amount of formic acid (10 drops) were then added. The reaction mixture was stirred for 15 hours at room temperature, during which a bright yellow precipitate formed. The suspension was vacuum filtered and the precipitate was washed with methanol (3 x 10 mL) and then with deionized (DI) water (3 x 10 mL). The precipitate was dried under vacuum to afford a bright yellow powder (14.63 g, 66.7% yield), which was used in the next step without further purification. ^{1}H NMR (400 MHz, chloroform-*d*) δ 8.11 (s, 2H), 6.92 (s, 4H), 2.30 (s, 6H), 2.17 (s, 12H). ^{13}C NMR (101 MHz, chloroform-*d*) δ 141.18, 139.31, 134.02, 130.59, 129.81, 124.61, 21.08, 17.56.

***N,N'*-(1,2-Ethanediylidene)bis-2,6-diisopropylphenylamine**

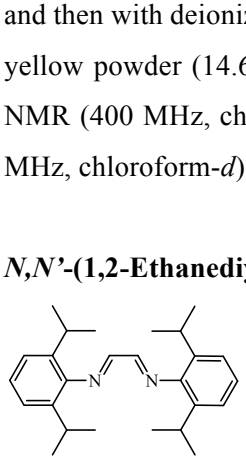

Following the procedure for ***N,N'*-(1,2-Ethanediylidene)bis-2,4,6-trimethylphenylamine** above. Briefly, a round-bottom flask was charged with 20 mL of methanol, to which was added 2,6-diisopropylaniline (3.77 mL, 20 mmol) and stirred until the primary amine had completely dissolved. To this solution was added

glyoxal (40% aqueous solution, 0.47 mL, 10 mmol) and a catalytic amount of formic acid (5 drops). The resulting solution turned brownish-yellow and was stirred at room temperature for 15 hours. The solution was vacuum filtered and the precipitate washed with methanol and DI water until the filtrate was clear. The precipitate was dried under vacuum to afford a yellow powder (703mg, 18.6% yield), which was used in the next step without further purification. ^{1}H NMR (400 MHz, chloroform-*d*) δ 8.11 (d, *J* = 1.9 Hz, 2H), 7.21 – 7.14 (m, 6H), 2.95 (sept, *J* = 6.9 Hz, 4H), 1.22 (d, *J* = 6.8 Hz, 24H). ^{13}C NMR (101 MHz, Chloroform-*d*) δ 163.07, 148.00, 136.68, 125.09, 123.15, 28.03, 23.36.

_N,N'_-(1,2-Ethanediylidene)bis-hydroxyphenylamine

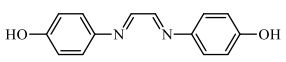

A round-bottom flask was charged with 20 mL of methanol, to this was added 4-aminophenol (813 mg, 7 mmol) and stirred until all of the primary amine was dissolved. To this solution was added glyoxal (40% aqueous solution, 0.14 mL, 3.0 mmol) and stirred for 5 hours at room temperature. After addition of glyoxal, the solution turned dark orange and precipitate was visible. The solution was vacuum dried and washed with methanol and ether. The precipitate was dried under vacuum to afford a brown powder (437 mg, 60.6% yield), which was used in the next step without further purification. ^{1}H NMR (400 MHz, DMSO-d_6) δ 9.76 (s, 2H), 8.40 (s, 2H), 7.32 (d, *J* = 8.0, 4H), 6.82 (d, *J* = 8.0, 4H). ^{13}C NMR (101 MHz, DMSO-d_6) δ 158.21, 156.85, 141.61, 123.77, 116.30.

1,3-Bis-mesitylimidazolium chloride (IMes·Cl), 2a

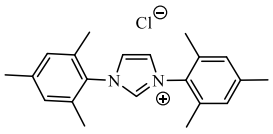

This procedure was adapted from that previously reported in the literature.[9] A round bottom flask charged with 30 mL of ethyl acetate and heated in an oil bath to 70 °C and *N,N'*-(1,2-Ethanediylidene)bis-2,4,6-trimethylphenylamine (2.00 g, 6.8 mmol) and paraformaldehyde (204 mg, 6.8 mmol) was added. Once all of the solids had completely dissolved, a solution of TMSCl (738.5 mg, 863 µL, 6.8 mmol) in ethyl acetate (850 µL) was added dropwise. After the addition of the TMSCl solution, a precipitate started to form. The reaction mixture was stirred for 2 hours at 70 °C then placed in cold refrigerator, 4 °C, overnight. The reaction mixture was vacuum filtered and washed with ethyl acetate (2 x 50 mL) and diethyl ether (2 x 50 mL). The solid was further dried under vacuum to afford the product as a tan/white powder (2.07 g, 89.3% yield). ^{1}H NMR (400 MHz, Chloroform-*d*) δ 10.85 (s, 1H), 7.61 (d, *J* = 1.7 Hz, 2H), 7.00 (s, 4H), 2.32 (s, 6H), 2.16 (s, 12H). ^{13}C NMR (101 MHz, Chloroform-*d*) δ 141.18, 139.31, 134.02, 130.59, 129.81, 124.61, 21.08, 17.56.

1,3-Bis-(2,6-diisopropylphenyl)imidazolium chloride (IDip·Cl), 2b

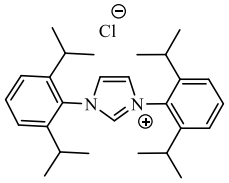

This procedure was adapted from that previously reported in the literature.[3] A round bottom flask charged with 10 mL of ethyl acetate was heated in an oil-bath to 70 °C and *N,N'*-(1,2-Ethanediylidene)bis-2,6-diisopropylphenylamine (400 mg, 1.06 mmol) and paraformaldehyde (31.8 mg, 1.06 mmol) were added. Once all of the solids had completely dissolved, a solution of TMSCl (115 mg, 150 µL, 1.06 mmol) in ethyl acetate (118 µL) was added dropwise with vigorous stirring. After the addition of the TMSCl solution, a precipitate started to form. The reaction mixture was stirred for 4 hours at 70 °C then placed in a cold refrigerator 4°C overnight. The solution was vacuum filtered and the precipitate washed with ethyl acetate (2 x 10 mL) and diethyl ether (2 x 10 mL). The precipitate was dried further under vacuum to afford the product as an off-white powder (210 mg, 46.7% yield). ^{1}H NMR (400 MHz, DMSO-d_6) δ 10.21 (s, 1H), 8.57 (d, J = 1.6 Hz, 2H), 7.69 (t, J = 8.0 Hz, 2H), 7.53 (d, J = 8.0 Hz, 4H), 2.35 (sept, J = 6.8 Hz, 4H), 1.26 (d, J = 4.0 Hz, 12H), 1.16 (d, J = 4.0 Hz, 12H). ^{13}C NMR (101 MHz, DMSO-d_6) δ 145.23, 139.75, 132.26, 130.48, 126.63, 125.04, 29.07, 24.54, 23.54.

1,3-Bis-(4-phenol)imidazolium chloride (IOH·Cl), 2c

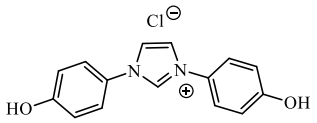

A round bottom flask charged with 30 mL of ethyl acetate was heated in an oil-bath to 70 °C and *N,N'*-(1,2-Ethanediylidene)bis-hydroxyphenylamine (600 mg, 3.6 mmol) and paraformaldehyde (108 mg, 3.6 mmol) were added. Once all the solids had completely dissolved, (ca. 30 minutes), a solution of TMSCl (391 mg, 600 µL, 3.6 mmol) in ethyl acetate (354 µL) was added dropwise. The reaction mixture was stirred for 2 hours at 70 °C after which the solution was placed in a cold refrigerator 4°C overnight. The reaction mixture was then vacuum filtered and washed with diethyl ether to afford the product as a brown powder (479.5 mg, 46.1% yield). ^{1}H NMR (400 MHz, DMSO-d_6) δ 10.35 (s, 2H), 10.10 (s, 1H), 8.40 (d, J = 4.0 Hz, 2H), 7.66 (d, J = 8.0 Hz, 4H), 7.01 (d, J = 12.0 Hz, 4H). ^{13}C NMR (101 MHz, DMSO-d_6) δ 159.27, 133.91, 126.76, 124.01, 122.31, 116.69.

1,3-Di-cyclohexylimidazolium tetrafluoroborate (ICy·BF_4), 2d

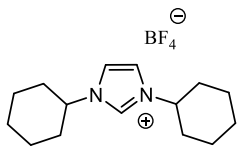

This procedure was modified from previously reported protocol.[9-10]A round-bottom flask was charged with 10 mL of toluene, to which paraformaldehyde (300 mg, 10 mmol) was added. Once all the solid had dissolved, cyclohexylamine was added (1.15 mL, 10 mmol) and cooled to 0 °C. To this solution was added a second equivalent of cyclohexylamine (1.15 mL, 10 mmol) and stirred for 10 minutes. Still at 0 °C, a solution of HBF_4 (50% in water, 1.63 mL,

12.5 mmol) was added dropwise with vigorous stirring. The solution was brought to room temperature and added a glyoxal solution 40% in water (1.14 mL, 10 mmol) slowly, turning the clear solution milky. The reaction mixture was then brought to 50 °C in an oil bath and stirred for 12 hours, after which it was vacuum filtered and dried. The crude solid was recrystallized from isopropanol to afford off-white needles (2.00 g, 62.7% yield). ^{1}H NMR (400 MHz, DMSO-d_6) δ 9.22 (s, 1H), 7.90 (d, J = 4.0 Hz, 2H), 4.25 (tt, J = 11.8, 3.8 Hz, 2H), 2.14 – 1.99 (m, 4H), 1.84 (dt, J = 13.4, 3.5 Hz, 4H), 1.68 (tdd, J = 12.1, 9.8, 3.6 Hz, 6H), 1.38 (qt, J = 12.9, 3.4 Hz, 4H), 1.20 (qt, J = 12.8, 3.5 Hz, 2H). ^{13}C NMR (101 MHz, DMSO-d_6) δ 133.87, 121.17, 59.15, 32.84, 24.93, 24.79.

Synthesis of 1,3-Di-tert-butylimidazolium tetrafluoroborate (ItBu·BF4), 2e

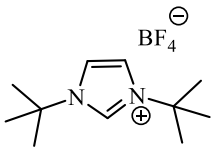

This procedure was adapted from previously reported protocol.[10] A round bottom flask was charged with 10 mL of toluene, to which was added paraformaldehyde (300 mg, 10 mmol), and stirred until all the solid had dissolved. To this solution was added tert-butylamine (1.06 mL, 10 mmol) with vigorous stirring. The resulting solution was cooled to 0 °C and a second equivalent of tert-butylamine (1.06 mL, 10 mmol) was added. With constant stirring, a solution of HBF_4 (50% in water, 2.04 mL, 10 mmol) was added dropwise. The solution was brought to room temperature and a glyoxal solution (40% aqueous in water 1.14 mL, 10 mmol) was added slowly. After addition of glyoxal, the solution turned milky white and a precipitate formed. The reaction mixture was stirred for 15 hours at room temperature and then vacuum filtered. The precipitate was washed with DI water and ether to afford an off-white solid (2.01 g, 75% yield). ^{1}H NMR (400 MHz, chloroform-*d*) δ 8.76 (s, 1H), 7.52 (s, 2H), 1.68 (s, 18H). ^{13}C NMR (101 MHz, chloroform-*d*) δ 120.06, 60.58, 29.56, 27.16.

Tetrabutylammonium acetylacetonate (NBu_4(acac))

The compound was made following the exact procedure previously reported in the literature. The title compound was stored at room temperature but showed decomposition over time. The title compound was made fresh prior to use. (600 mg, 87.8% yield).[11]

Dichloro(1,10-phenanthroline)gold(III) chloride ([Au(phen)Cl_2]NO_3)

This procedure was adapted from previous reports in the literature.[12] To a round bottom flask charged with 15 mL of ethanol was added $HAuCl_4 \cdot 3H_2O$ (393 mg, 1 mmol) followed by phenanthroline monohydrate (495 mg, 2.5 mmol). Upon addition of phenanthroline, a yellow precipitate formed. The suspension was then refluxed for 4 hours, the resulting orange precipitate was filtered and dissolved in water (10 mL) and to this solution was added conc. HNO_3 (10 drops) to form the title compound as a yellow solid. (412 mg,

76% yield). ^{1}H NMR (400 MHz, DMSO-d_6) δ 9.71 (d, J = 4.0 Hz, 2H), 9.35 (d, J = 8.0 Hz, 2H), 8.53 (s, 2H), 8.45 (dd, J = 10, 4 Hz, 2H).

Trichloro(2-benzoylpyridine)gold(III) (Au(Bzpy)Cl_3)

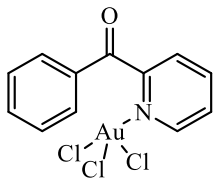

2-benzoylpyridine (1.00 g, 5.46 mmol) and $HAuCl_4 \cdot 3H_2O$ (1.07 g, 2.73 mmol) were each dissolved in ethanol (20 mL). The two solutions were then added into a single 100 ml round-bottom flask with a magnetic stir bar. After several minutes of stirring, a yellow precipitate formed. The reaction mixture was stirred for 14 hours at room temperature. The precipitate was then vacuum filtered and washed with diethyl ether to afford a yellow solid (963.0 mg, 72.5% yield), which could then be used without further purification. ^{1}H NMR (400 MHz, DMSO-d_6) δ 8.75 – 8.70 (m, 1H), 8.08 (t, J = 7.7 Hz, 1H), 8.02 – 7.93 (m, 3H), 7.68 (t, J = 7.1 Hz, 2H), 7.55 (t, J = 7.6 Hz, 2H).

Dichloro(2-benzoylpyridine)gold(III) (Au(Bzpy)Cl_2) [1][13]

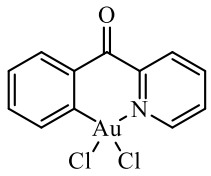

Trichloro(2-benzoylpyridine)gold (2.00 g, 4.11 mmol) was dissolved in 75 ml of acetonitrile. Silver nitrate (698 mg, 4.11 mmol) was then added to a round-bottom flask charged with acetonitrile (75 mL) and sonicated until all of the silver nitrate had dissolved. The silver nitrate solution was added to the trichloro(2-benzolypyridine)gold(III) solution equipped with a magnetic stir bar and refluxed at 95 °C for 16 hours. The reaction mixture was filtered while hot and the filtrate was then slowly cooled with nitrogen to a minimum volume and sonicated for several minutes (15 min) to enhance precipitate formation. The solid was vacuum filtered and dried to afford a white solid. The filtrate was then recycled back into reflux for an additional 10 hours and subjected to the same workup mentioned above. The solids were combined and washed with diethyl ether and dried under vacuum to afford a white solid (856.7 mg, 46.31% yield), which could be used without further purification. ^{1}H NMR (400 MHz, DMSO-d_6) δ 9.48 (d, J = 6.1 Hz, 1H), 8.56 (t, J = 8.3, 1H), 8.37 (d, J = 7.8, 1H), 8.09 (t, J = 7.5, 1H), 7.76 (d, J = 9.1, 1H), 7.69 (d, J = 9.3, 1H), 7.54 – 7.42 (m, 2H). ^{13}C NMR (101 MHz, DMSO-d_6) δ 188.63, 152.69, 145.09, 144.29, 136.71, 133.88, 133.16, 129.81, 129.52, 128.54, 127.74, 127.03. LRMS (ESI) (m/z): calcd for $C_{12}H_8AuCl_2NO$ [M+] 448.96, found: 449.00.

Dichloro(2-benzylpyridine)gold(III) [1'][14]

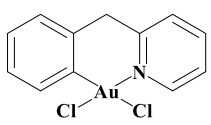

In a 100 ml round-bottom flask, 2-benzylpyridine (1.00 g, 5.91 mmol) and $HAuCl_4 \cdot 3H_2O$ (1.07 g, 2.73 mmol) were dissolved in distilled water (20 mL). The reaction mixture was stirred for 8 hours at 140 °C. The precipitate was then vacuum

filtered and washed with water to afford an off-white solid (952.0 mg, 80 % yield), which could then be used without further purification. ^{1}H NMR (400 MHz, DMSO-d_6) δ 9.17 (d, J = 6.1 Hz, 1H), 8.26 (t, J = 7.7 Hz, 1H), 7.99 (d, J = 7.8 Hz, 1H), 7.70 (t, J = 7.6 Hz, 1H), 7.41 (d, J = 8.0 Hz, 1H), 7.25 (d, J = 7.4 Hz, 1H), 7.18 (t, J = 7.3 Hz, 1H), 7.07 (t, J = 7.6 Hz, 1H), 4.61 (d, J = 15.2 Hz, 1H), 4.34 (d, J = 15.3 Hz, 1H). ^{13}C NMR (101 MHz, DMSO-d_6) δ 155.66 , 152.06 , 143.26 , 141.08 , 132.70 , 131.94 , 128.61 , 127.95 , 126.92 , 126.39 , 124.48 , 46.07.

Model reactions for reductive elimination of C – N bond formation and Au(I) complexes

Au(IMes)Cl (4a)

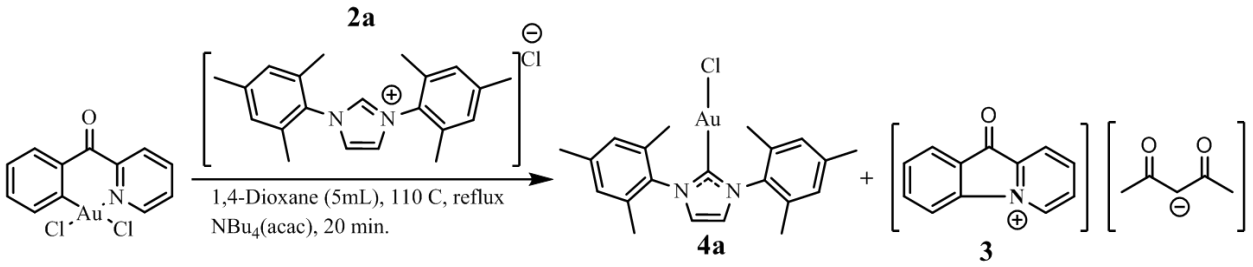

Reaction using $NaHCO_3$(s)

Under normal atmospheric conditions, dichloro(2-benzoylpyridine)gold(III), **1** (29 mg, 0.06 mmol) and **2a** (22 mg, 0.06 mmol) were dissolved in 5 ml of acetonitrile with $NaHCO_3$(s) (11 mg, 0.13 mmol). The solution was stirred and refluxed at 82 °C for 44 hours. The color changed from pale yellow to dark green and the reaction solution was monitored by TLC in 5% MeOH - DCM. The title compound had an Rf ~ 0.9. The product was separated by flash silica-gel column chromatography using 5 % MeOH in DCM as eluent via isocratic elution (Yield: ~5.0 mg, 14 %). ^{1}H NMR (400 MHz, Methylene Chloride-d_2) δ 7.16 (s, 1H), 7.07 (s, 2H), 2.38 (s, 3H), 2.13 (s, 6H)

Reaction using t-BuOK(s)

Under normal atmospheric conditions, dichloro(2-benzoylpyridine)gold(III), **1** (20 mg, 0.05 mmol) and **2a** (18 mg, 0.06 mmol) were dissolved in 5 ml of acetonitrile with t-BuOK (22 mg, 0.06 mmol). The solution was stirred and refluxed at 82 °C for 2 h. The color changed from pale yellow to dark green and the reaction solution was monitored by TLC in 5% MeOH - DCM. The title compound had an Rf ~ 0.9. The product was separated by flash silica-gel column chromatography using 5 % MeOH in DCM as eluent via isocratic elution (Yield: 6 mg, 22 %). ^{1}H NMR (400 MHz, acetonitrile-d_3) δ 7.36 (s, 2H), 7.11 (s, 4H), 2.37 (s, 6H), 2.11 (s, 12H); ^{13}C NMR (101 MHz, chloroform-*d*): δ 173.29, 139.73, 134.64, 134.59, 129.44, 122.13, 21.11, 17.73.

Au(IDip)Cl (4b)

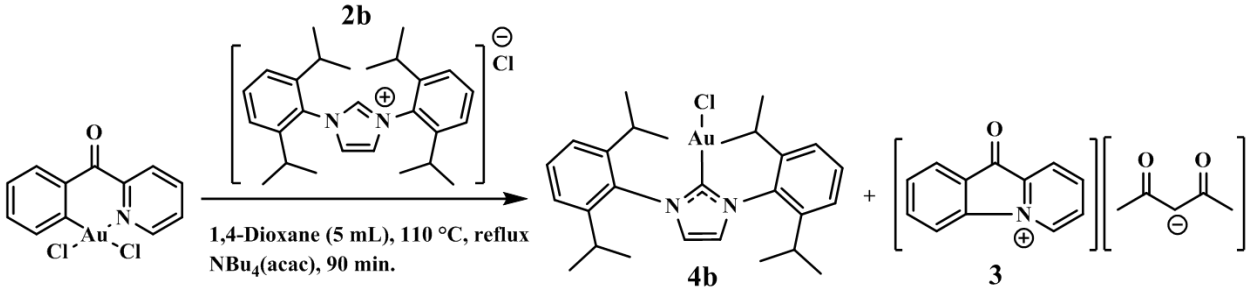

Au(IOH)Cl (4c)

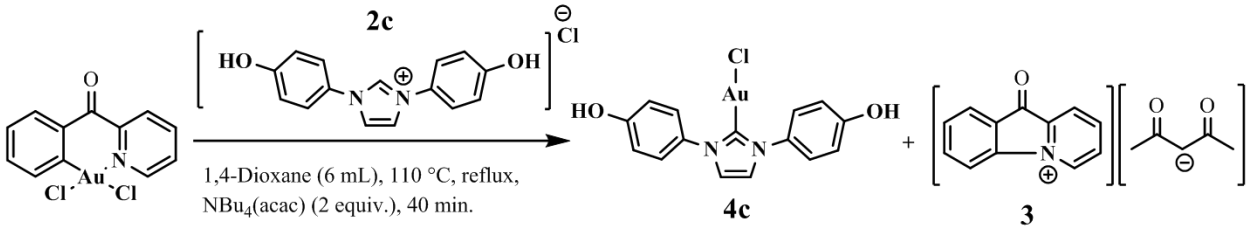

Au(ICy)BF_4 (4d)

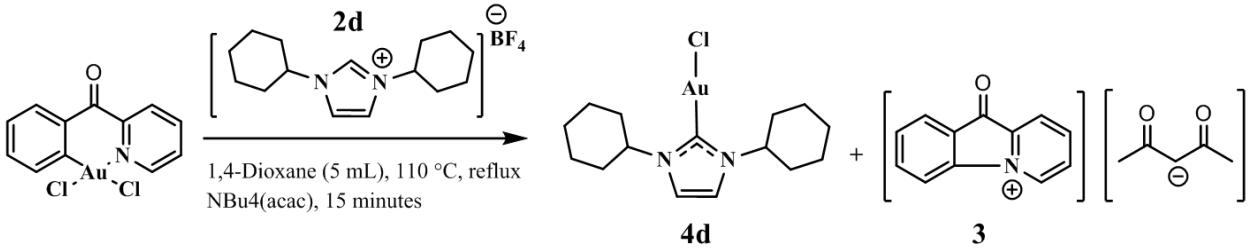

Au(ItBu)BF_4 (4e)

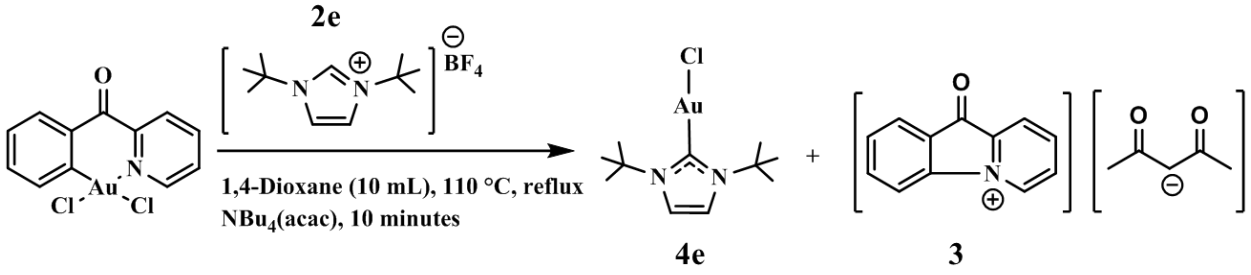

Au(IDip)Cl (4'b) with 1'

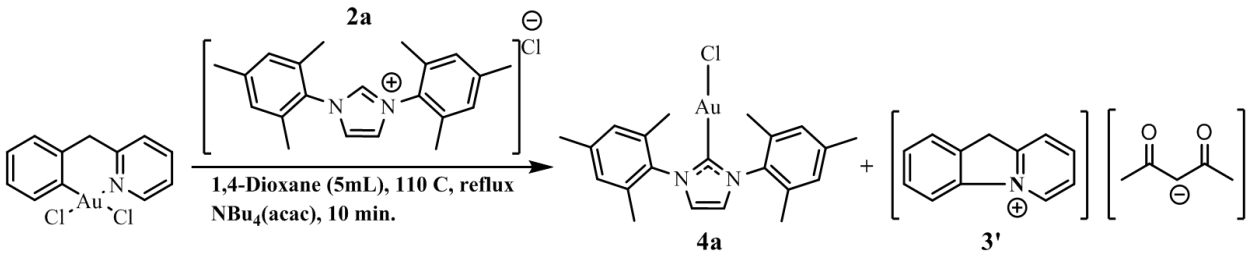

Au(IOH)Cl (4c) with 1'

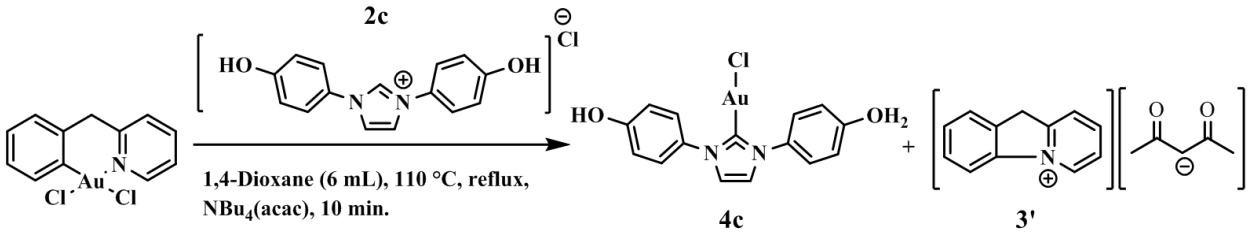

Au(ICy)BF_4 (4d) with 1'

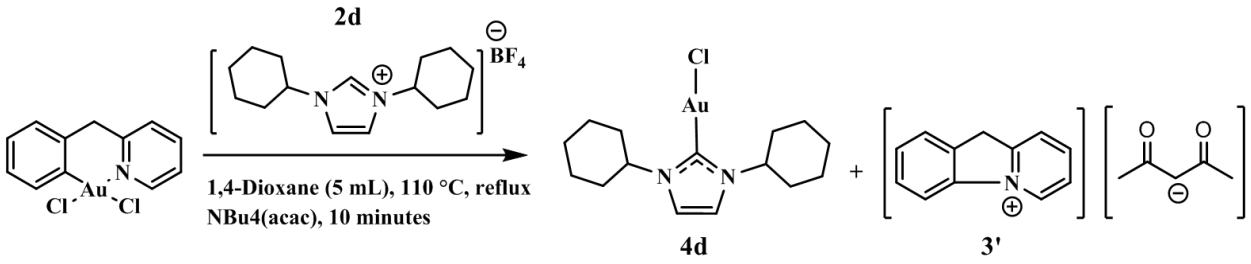

Au(ItBu)BF_4 (4e) with 1'

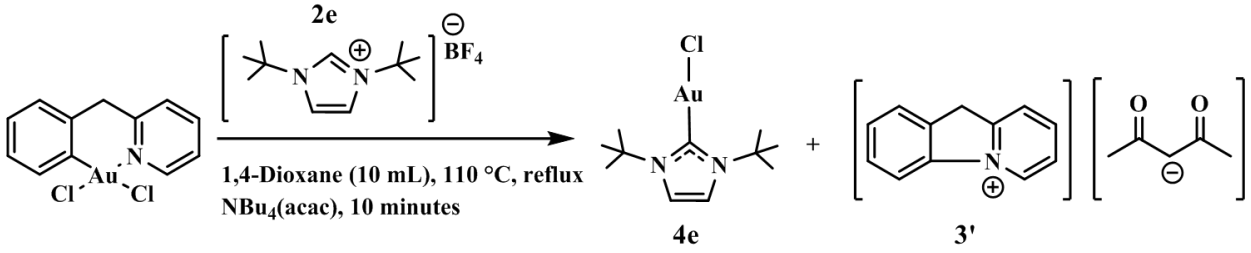

Reaction of 1 + 2f

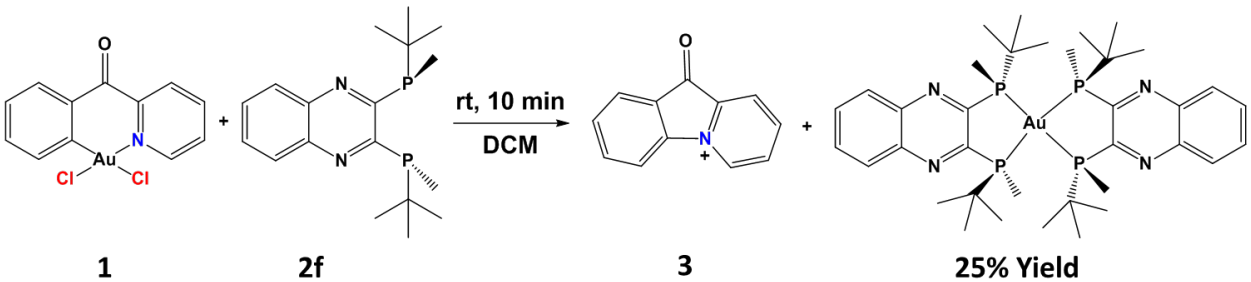

NMR Spectra Data

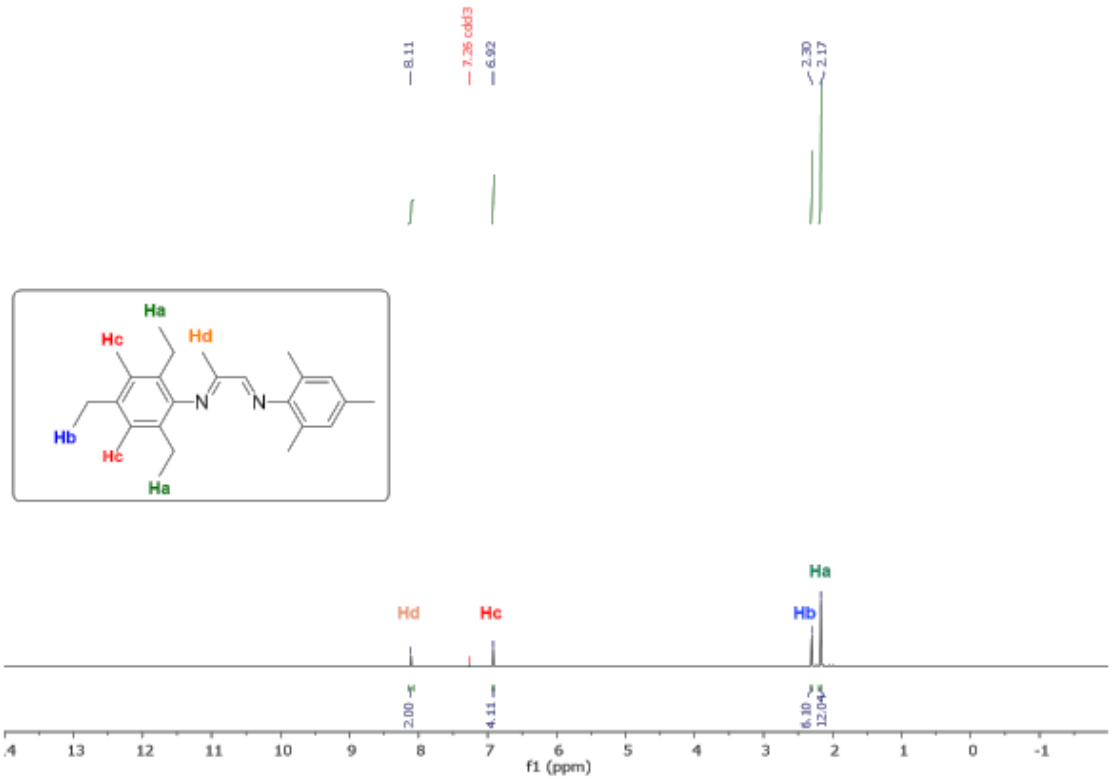

Figure S1. ^{1}H NMR spectrum of *N,N'*-(1,2-Ethanediylidene)bis-2,4,6-trimethylphenylamine ($CDCl_3$, 298K)

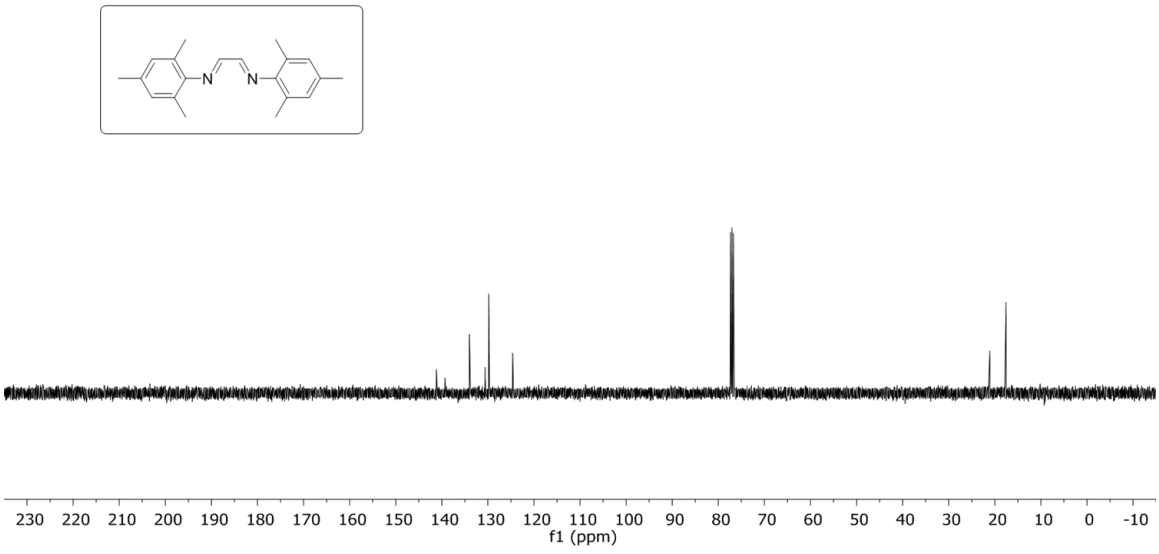

Figure S2. ^{13}C{^{1}H} NMR spectrum of *N,N'*-(1,2-Ethanediylidene)bis-2,4,6-trimethylphenylamine ($CDCl_3$, 298K)

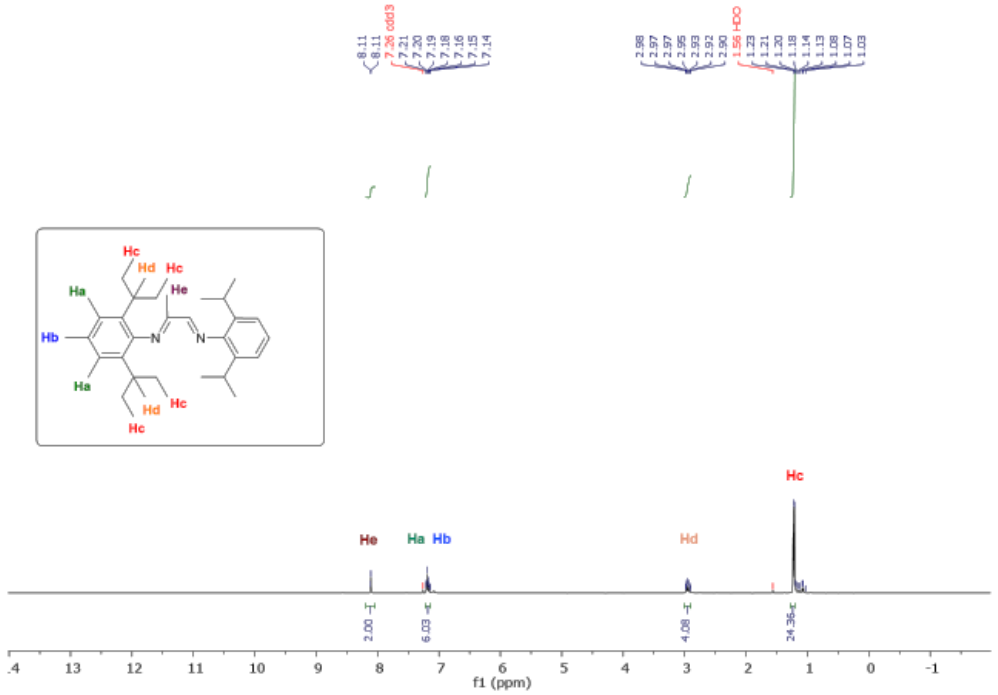

Figure S3. ^{1}H NMR spectrum of *N,N'*-(1,2-Ethanediylidene)bis-2,6-diisopropylphenylamine ($CDCl_3$, 298K)

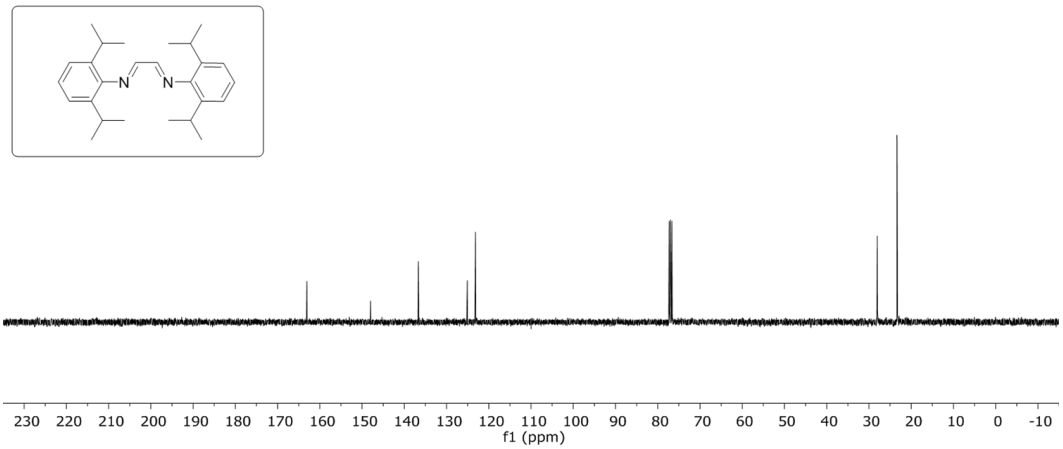

Figure S4. $^{13}C\{^{1}H\}$ NMR spectrum of *N,N'*-(1,2-Ethanediylidene)bis-2,6-diisopropylphenylamine ($CDCl_3$, 298K)

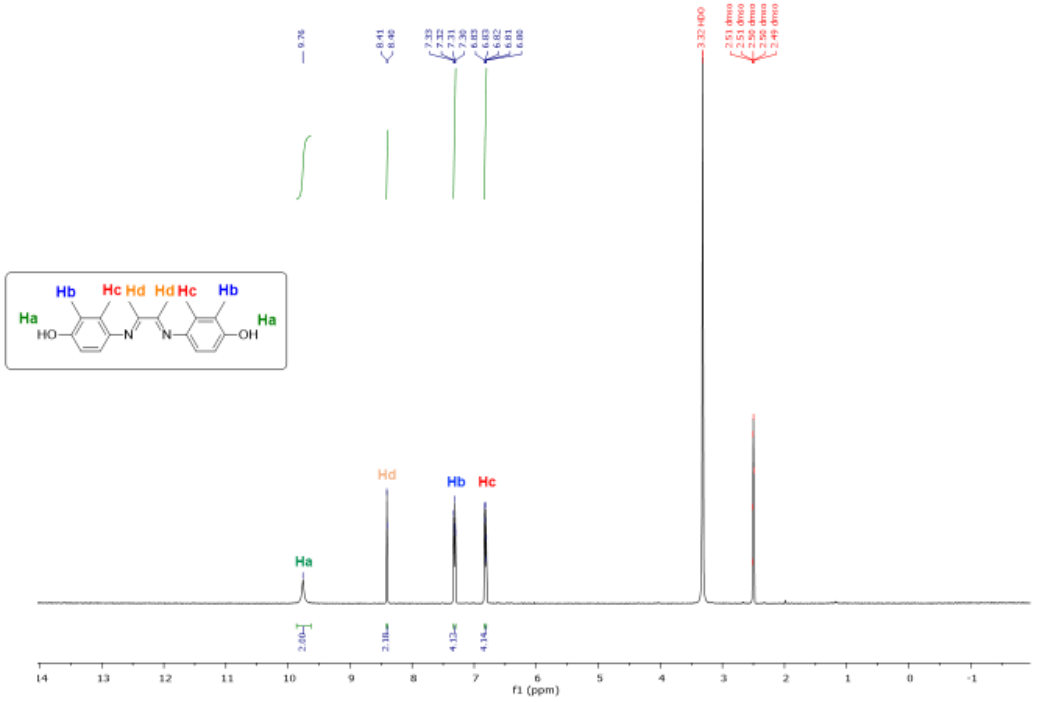

Figure S5. ^{1}H NMR spectrum of *N,N'*-(1,2-Ethanediylidene)bis-hydroxyphenylamine (DMSO-d_6, 298K)

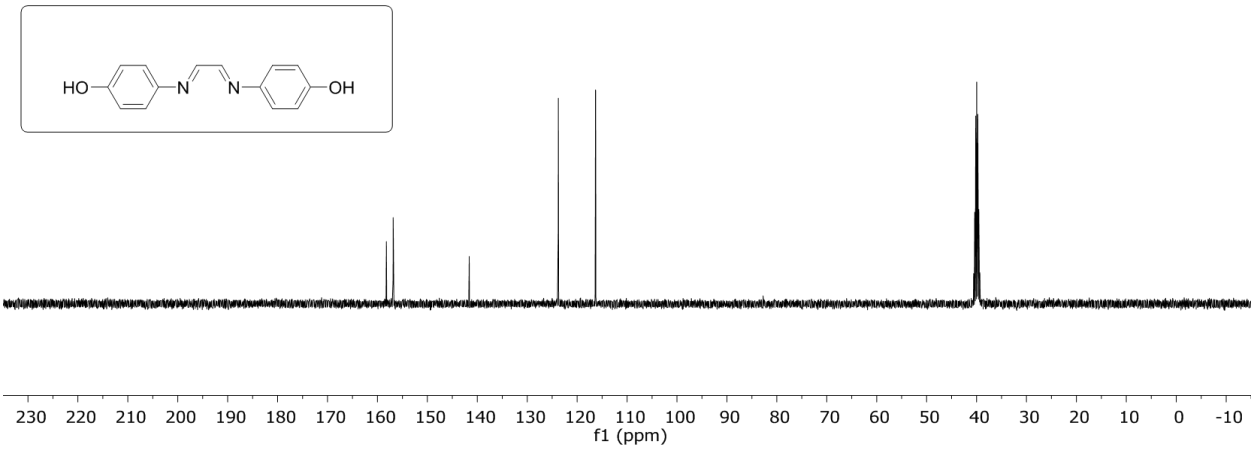

Figure S6. ^{13}C{^{1}H} NMR spectrum of *N,N'*-(1,2-Ethanediylidene)bis-hydroxyphenylamine (DMSO-d_6, 298K)

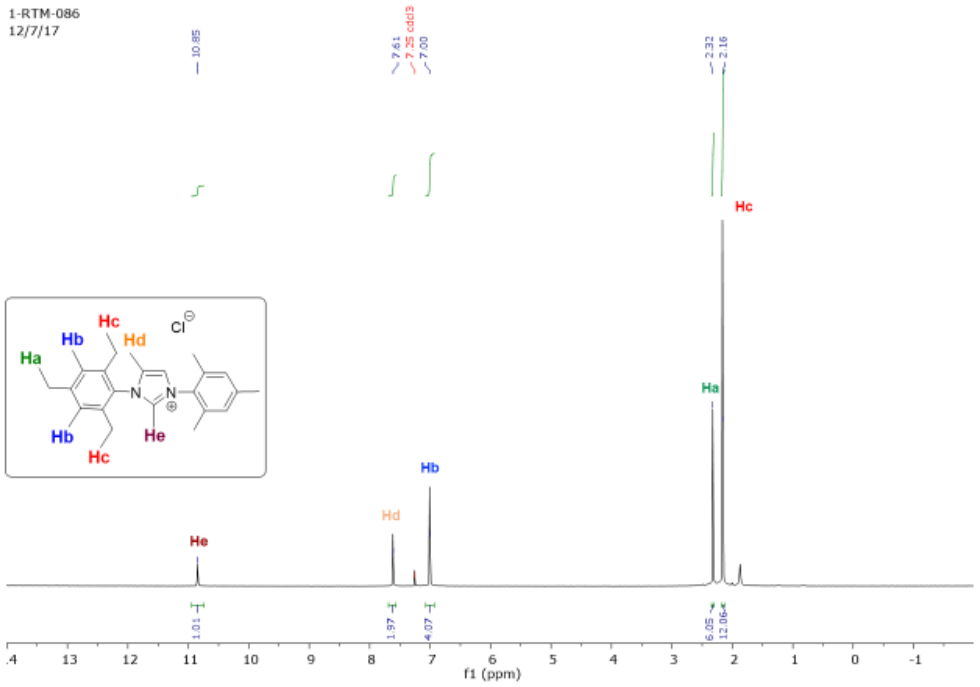

Figure S7. ^{1}H NMR spectrum of 1,3-Bis-mesitylimidazolium chloride (IMes·Cl), **2a** ($CDCl_3$, 298K)

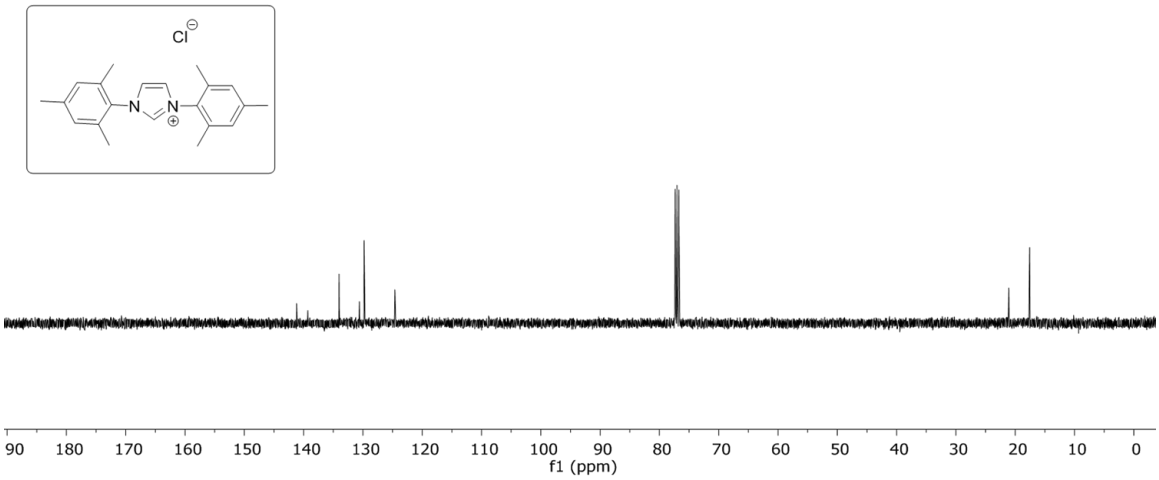

Figure S8. $^{13}C\{^{1}H\}$ NMR spectrum of 1,3-Bis-mesitylimidazolium chloride (IMes·Cl), **2a** ($CDCl_3$, 298K)

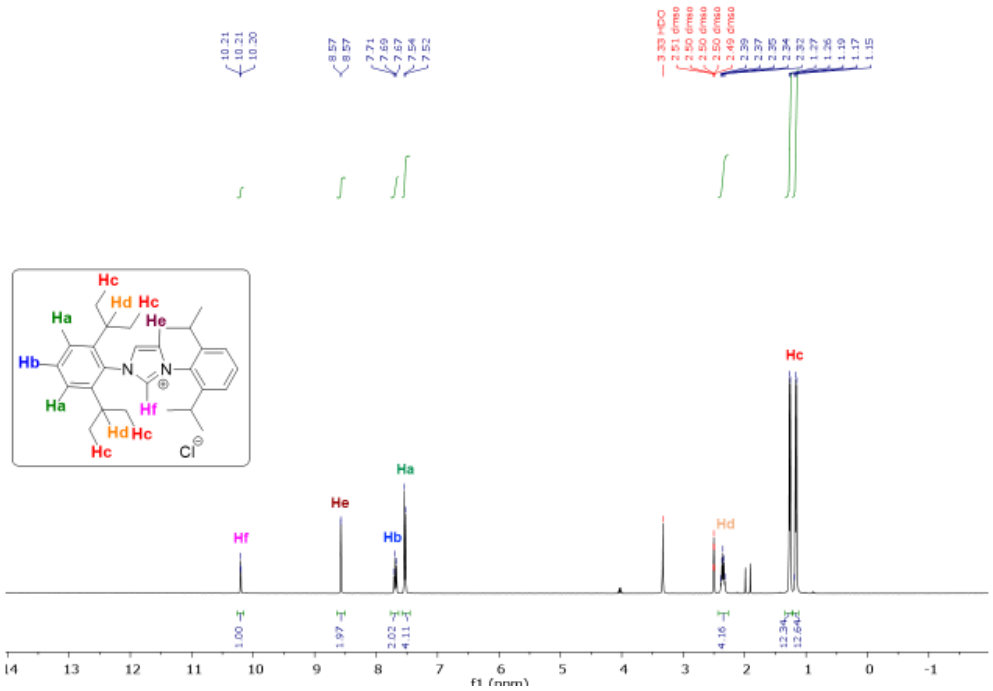

Figure S9. ^{1}H NMR spectrum of 1,3-Bis-(2,6-diisopropylphenyl)imidazolium chloride (IDip·Cl), **2b** (DMSO-d_6, 298K)

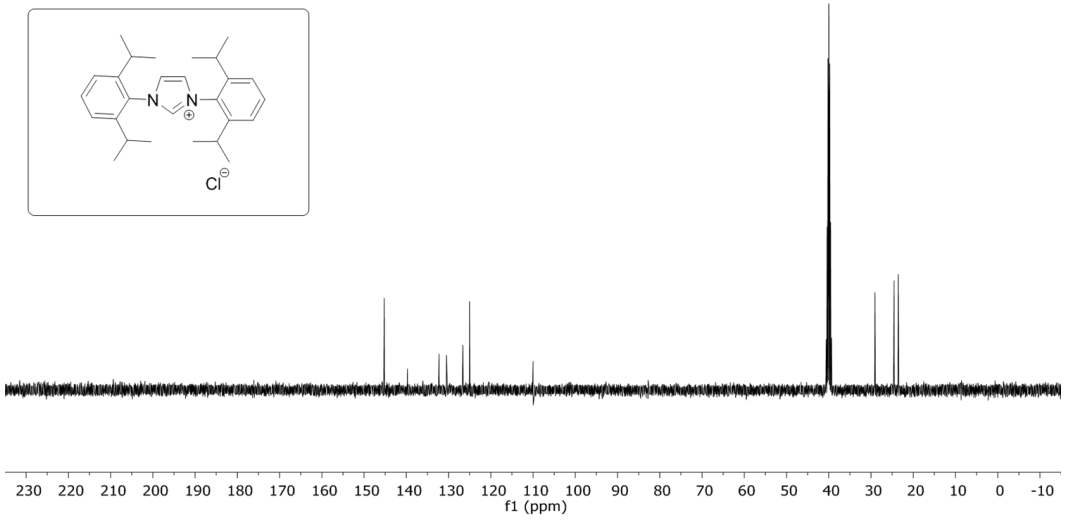

Figure S10. ^{13}C{^{1}H} NMR spectrum of 1,3-Bis-(2,6-diisopropylphenyl)imidazolium chloride (IDip·Cl), **2b** (, DMSO-d_6, 298K)

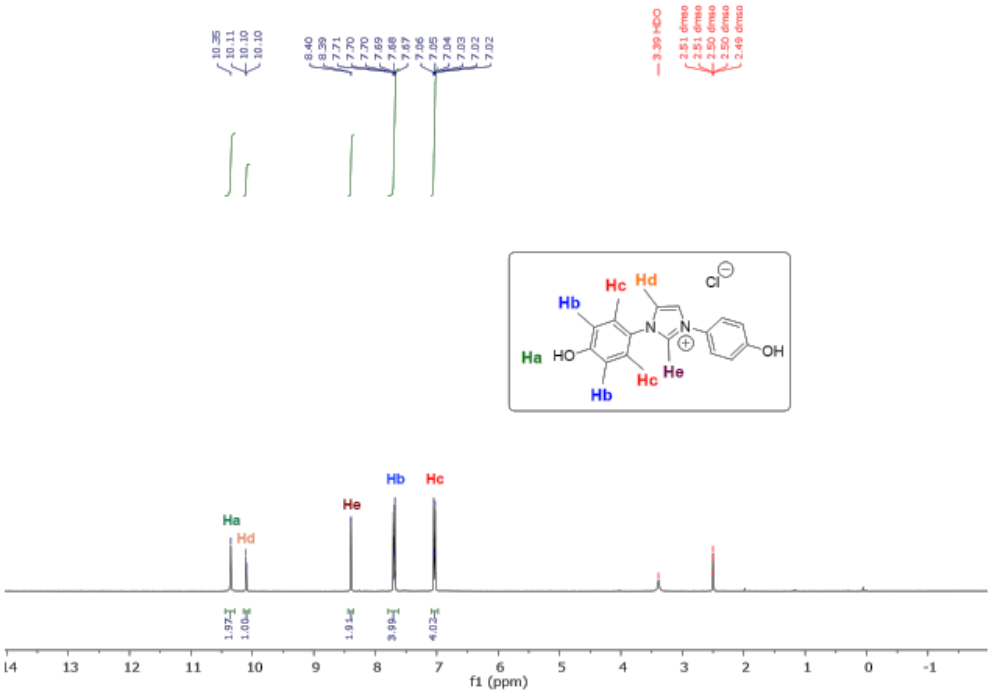

Figure S11. ^{1}H NMR spectrum of 1,3-Bis-(4-phenol)imidazolium chloride (IOH·Cl), **2c** (DMSO-d_6, 298K)

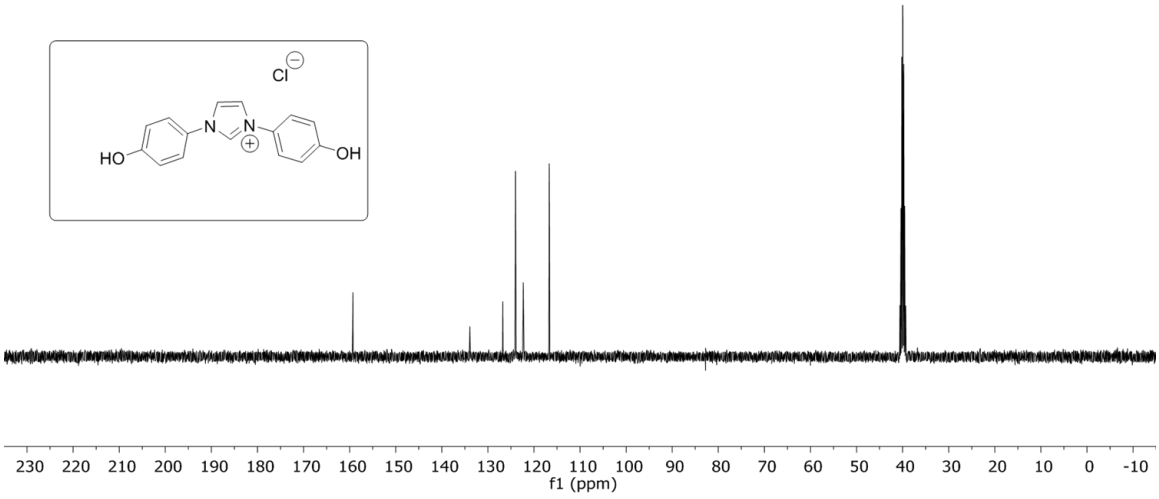

Figure S12. ^{13}C{^{1}H} NMR spectrum of 1,3-Bis-(4-phenol)imidazolium chloride (IOH·Cl), **2c** (DMSO-d_6, 298K)

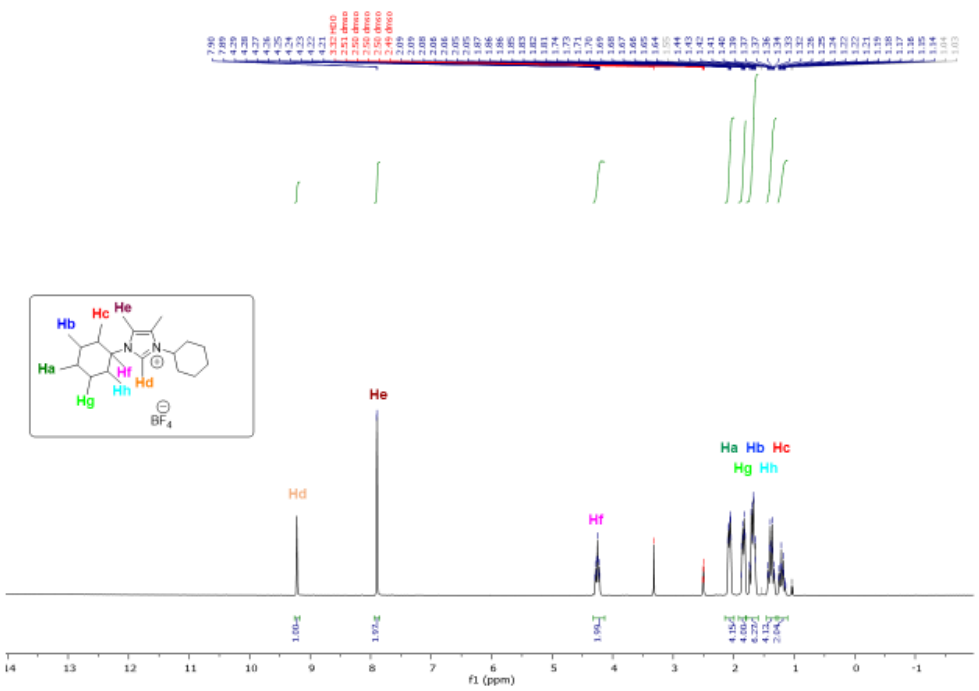

Figure S13. ^{1}H NMR spectrum of 1,3-Di-cyclohexylimidazolium tetrafluoroborate (ICy·BF4), **2d** (DMSO-d_6, 298K)

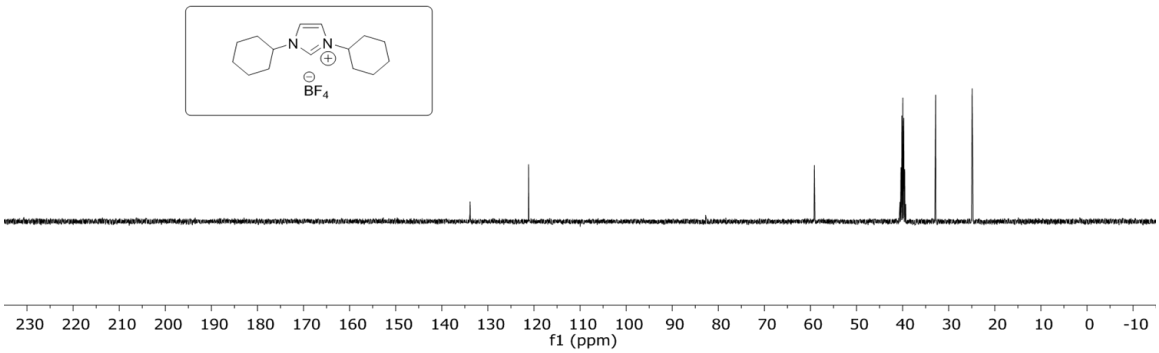

Figure S14. ^{13}C{^{1}H} NMR spectrum of 1,3-Di-cyclohexylimidazolium tetrafluoroborate (ICy·BF4), **2d** (DMSO-d_6, 298K)

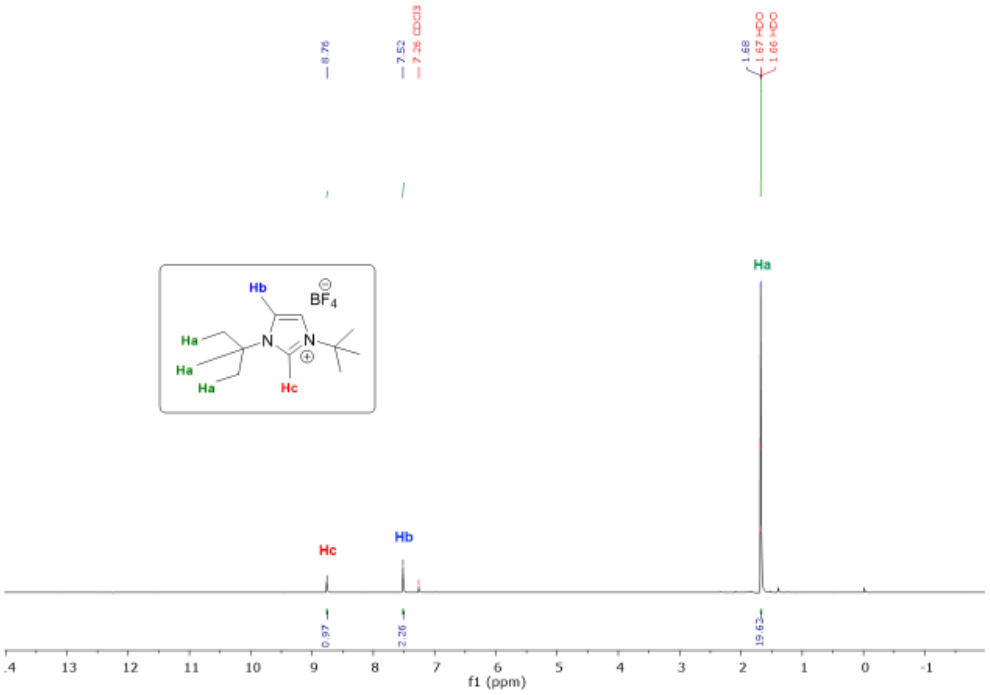

Figure S15. ^{1}H NMR spectrum of 1,3-Di-tert-butylimidazolium tetrafluoroborate (ItBu·BF4), **2e** ($CDCl_3$, 298K)

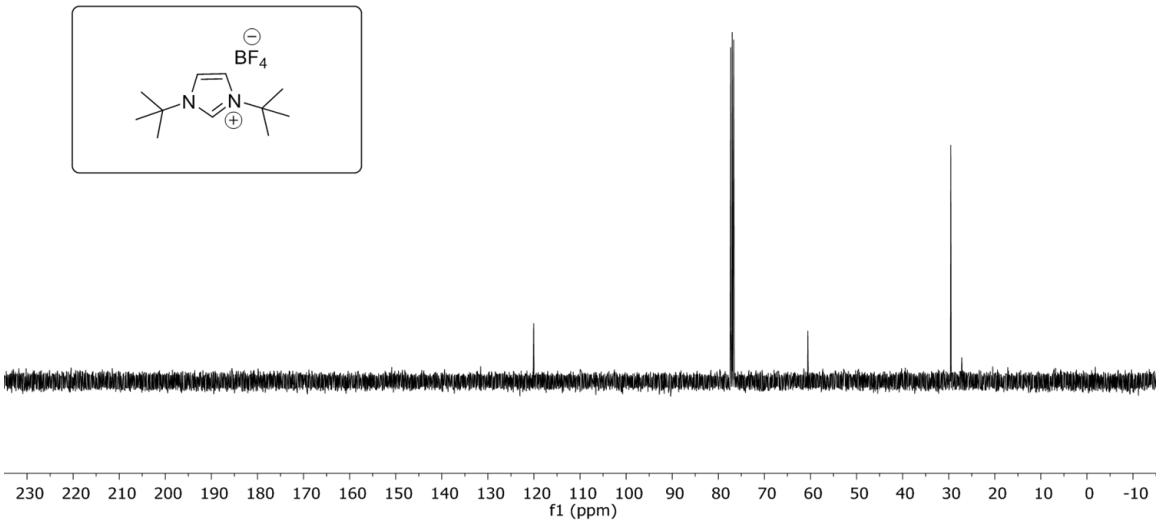

Figure S16. $^{13}C\{^{1}H\}$ NMR spectrum of 1,3-Di-tert-butylimidazolium tetrafluoroborate (ItBu·BF4), **2e** ($CDCl_3$, 298K)

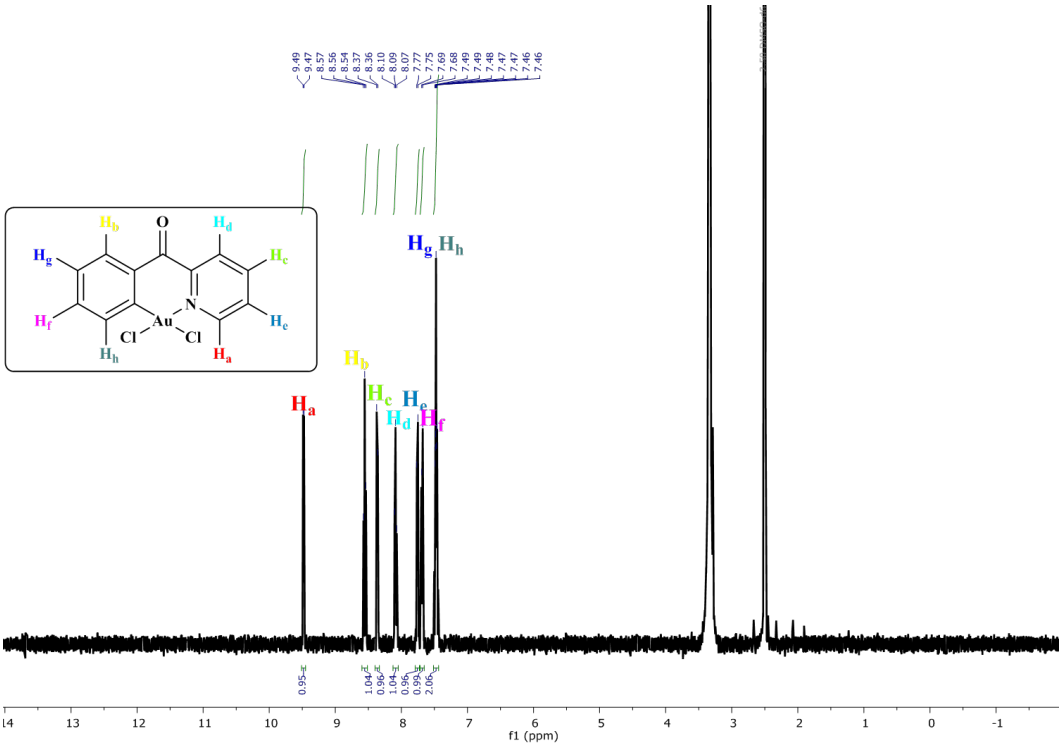

Figure S17. ^{1}H NMR spectrum of cyclometalated Au(III) (**1**) (DMSO, 298K)

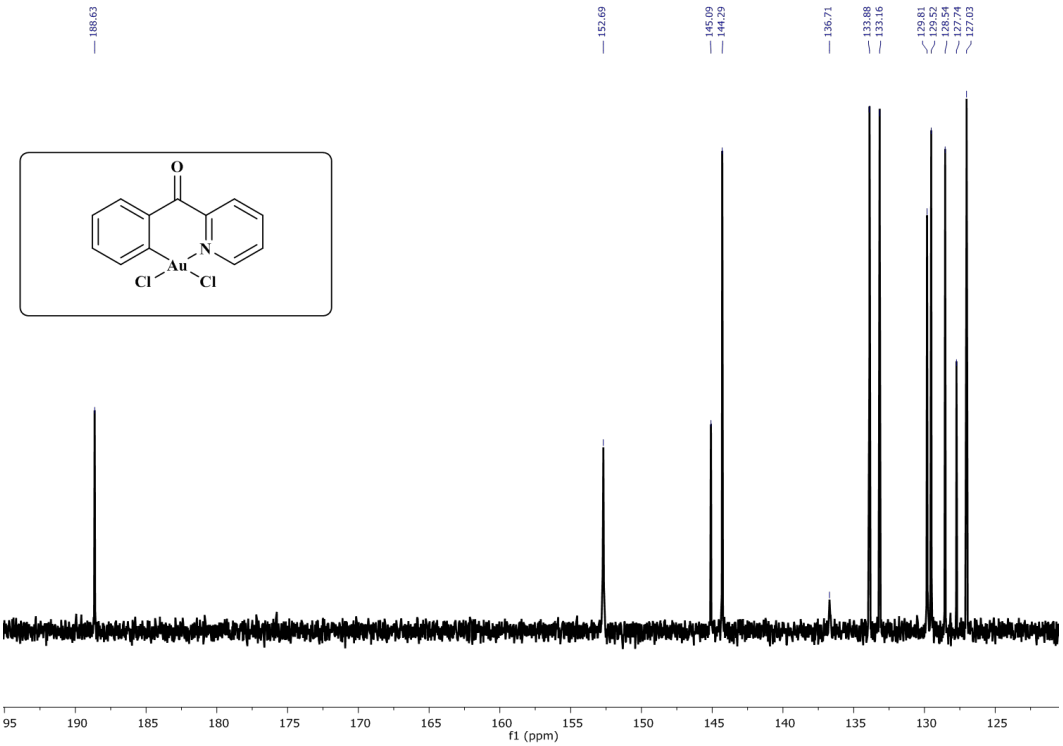

Figure S18. ^{13}C{^{1}H} NMR spectrum of cyclometalated Au(III) (**1**) (DMSO, 298K)

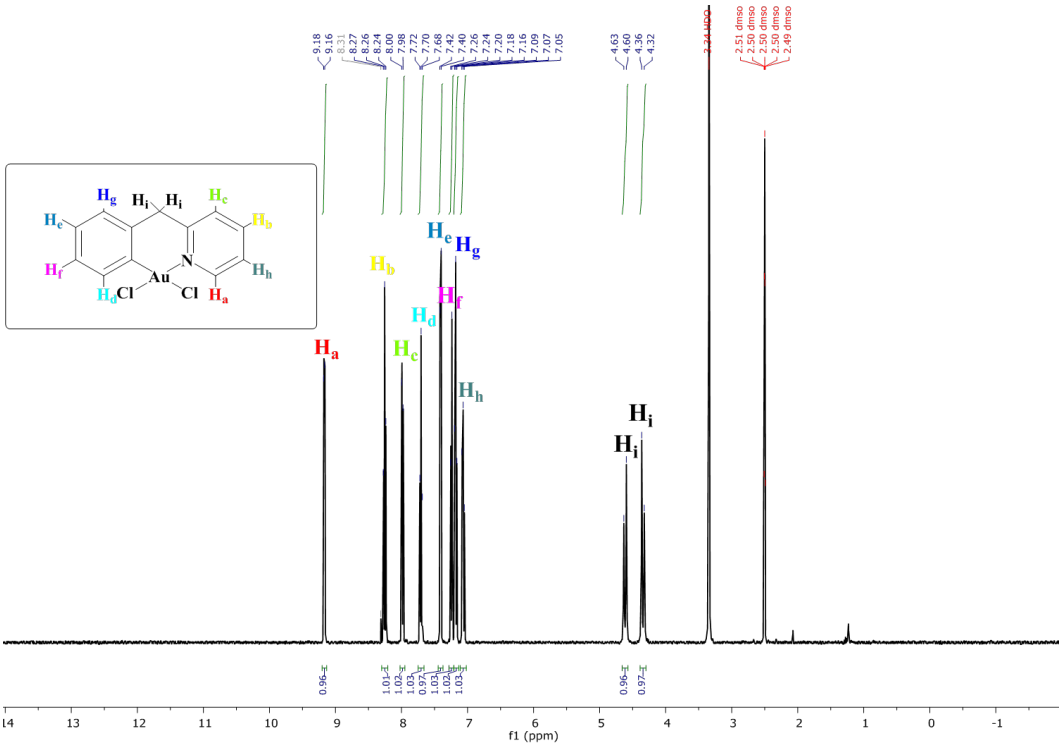

Figure S19. ^{1}H NMR spectrum of cyclometalated Au(III) (**1'**) (DMSO, 298K)

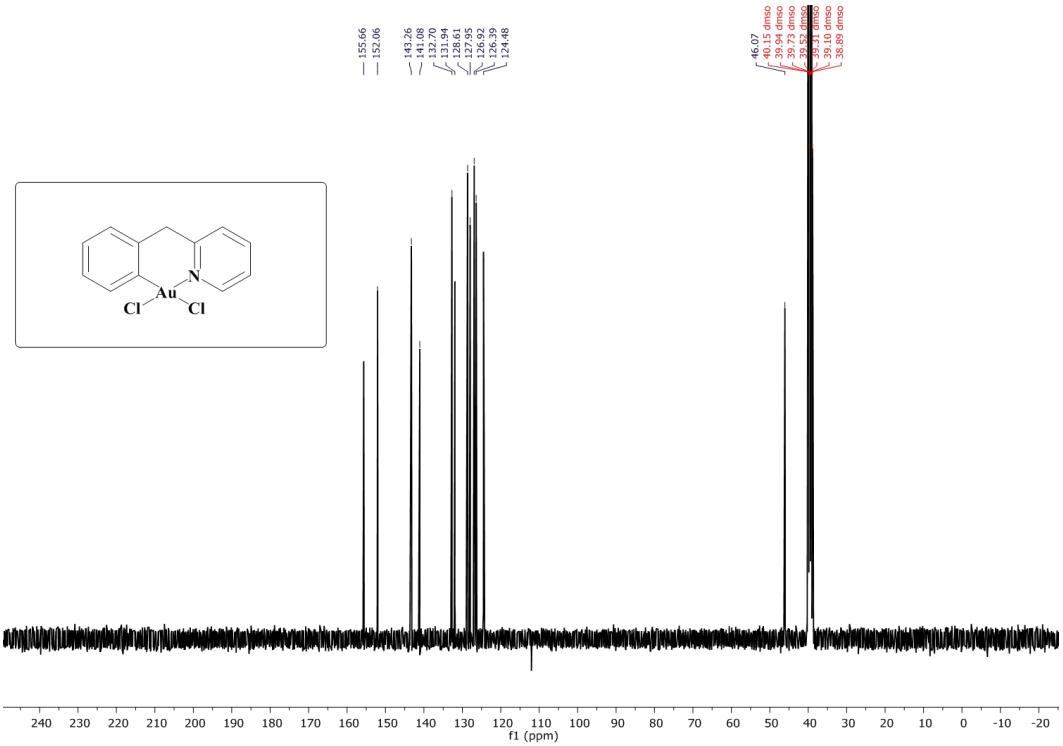

Figure S20. $^{13}C\{^{1}H\}$ NMR spectrum of cyclometalated Au(III) (**1'**) (DMSO, 298K)

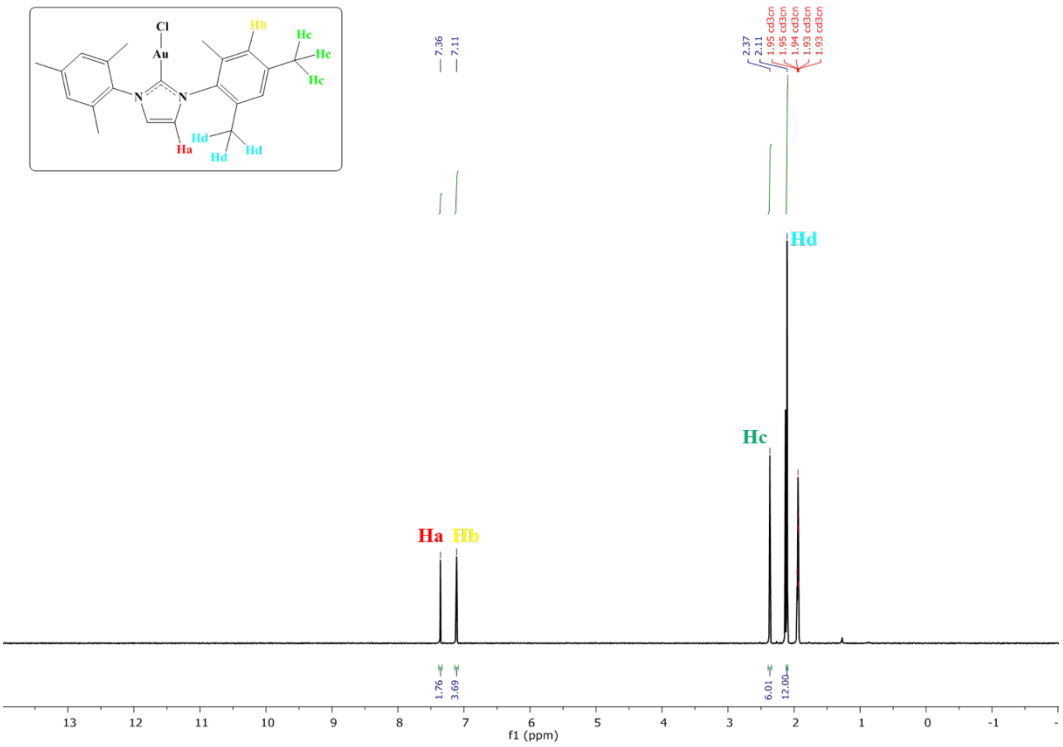

Figure S21. ^{1}H NMR spectrum of complex **4a** ($CDCl_3$, 298K)

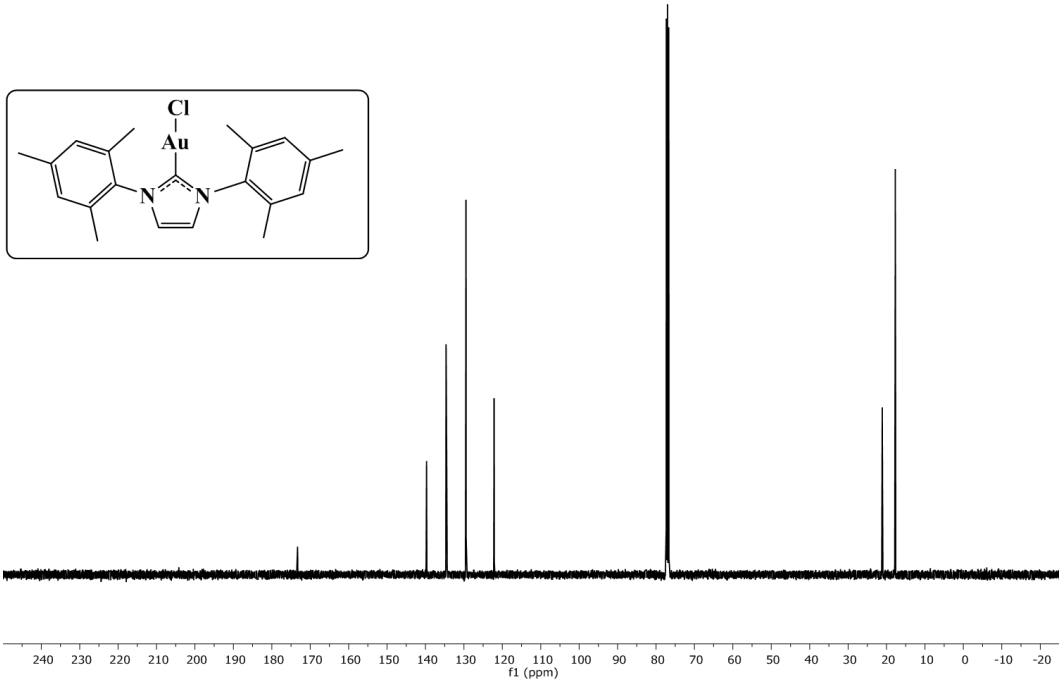

Figure S22. $^{13}C\{^{1}H\}$ NMR spectrum of complex **4a** ($CDCl_3$, 298K)

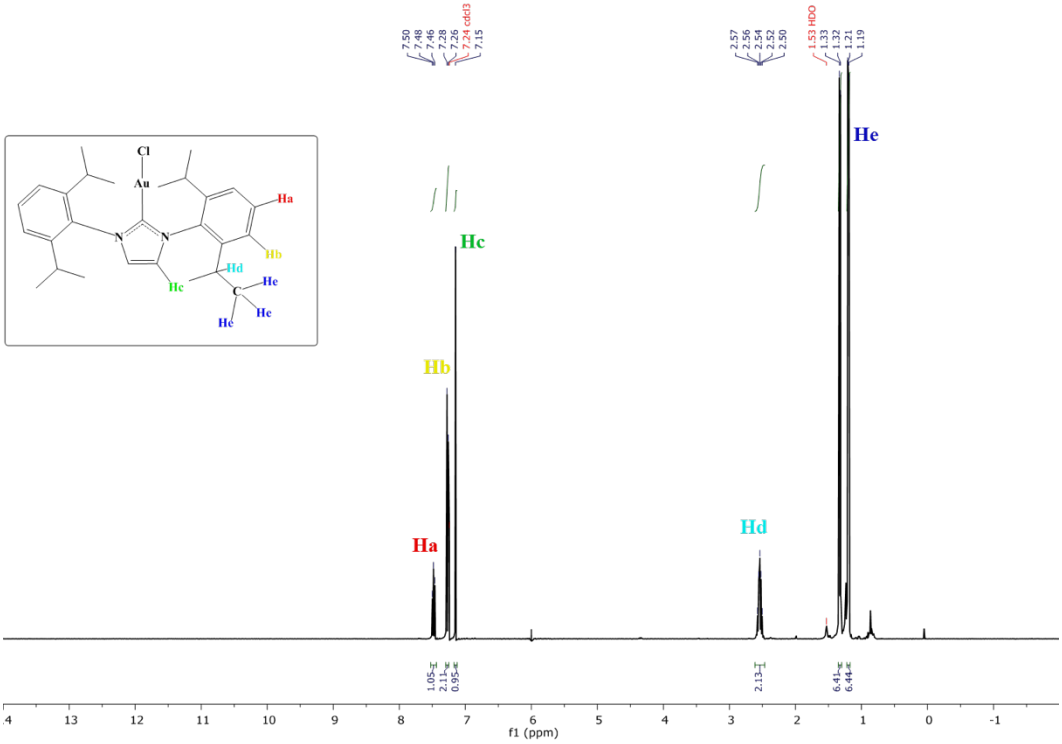

Figure S23. ^{1}H NMR spectrum of complex **4b** ($CDCl_3$, 298K)

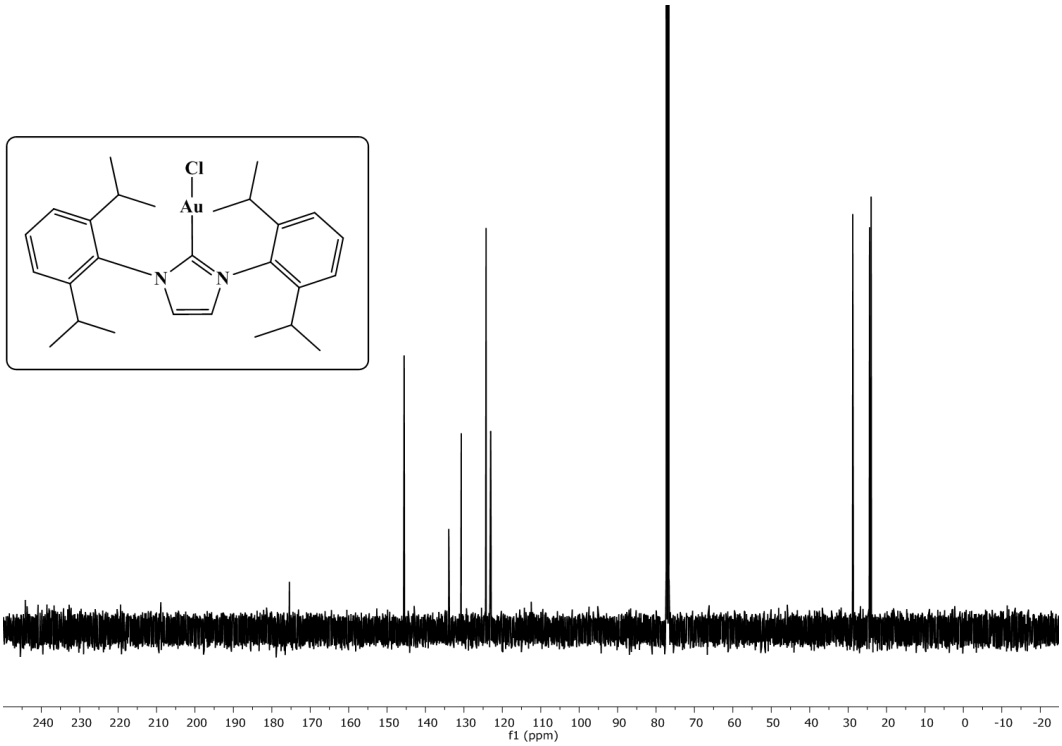

Figure S24. $^{13}C\{^{1}H\}$ NMR spectrum of complex **4b** ($CDCl_3$, 298K)

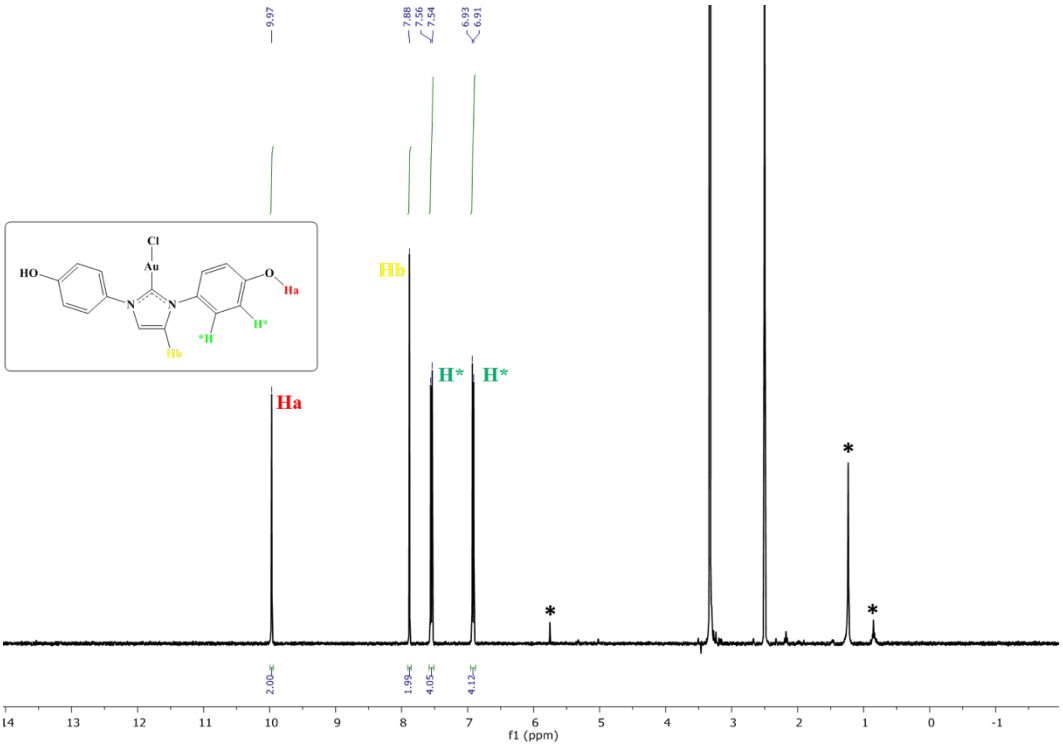

Figure S25. ^{1}H NMR spectrum of complex **4c** (DMSO-d_6, 298K). * dichloromethane and grease respectively.

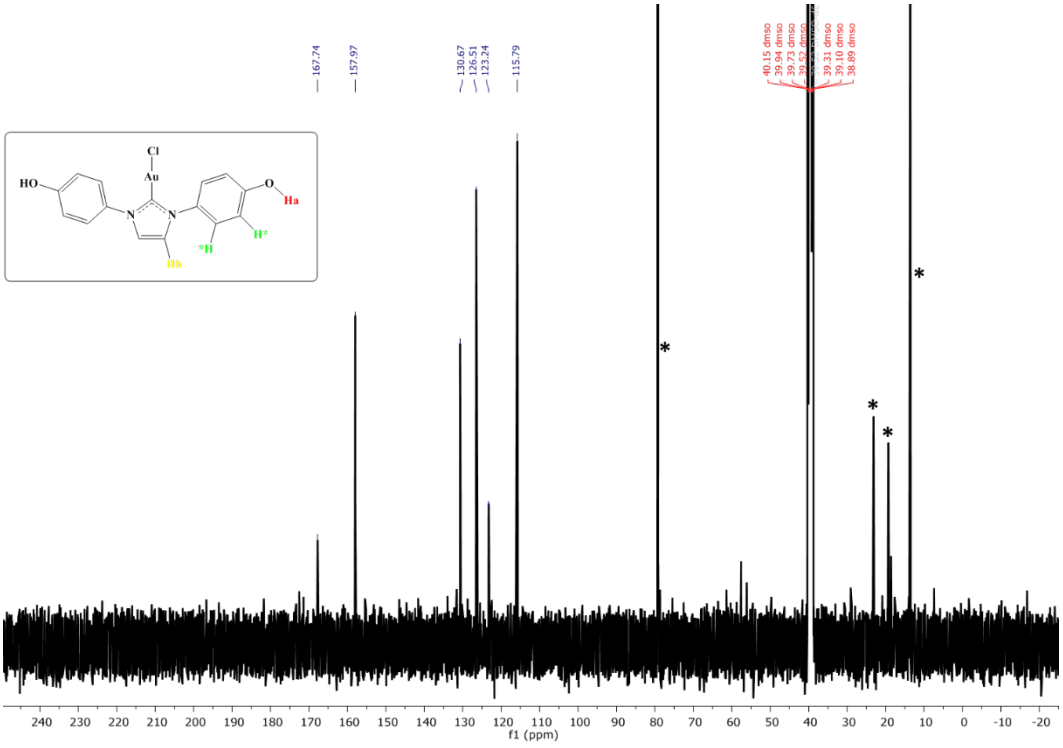

Figure S26. ^{13}C{^{1}H} NMR spectrum of complex **4c** (DMSO-d_6, 298K) * Chloroform (79.22 ppm) and grease.

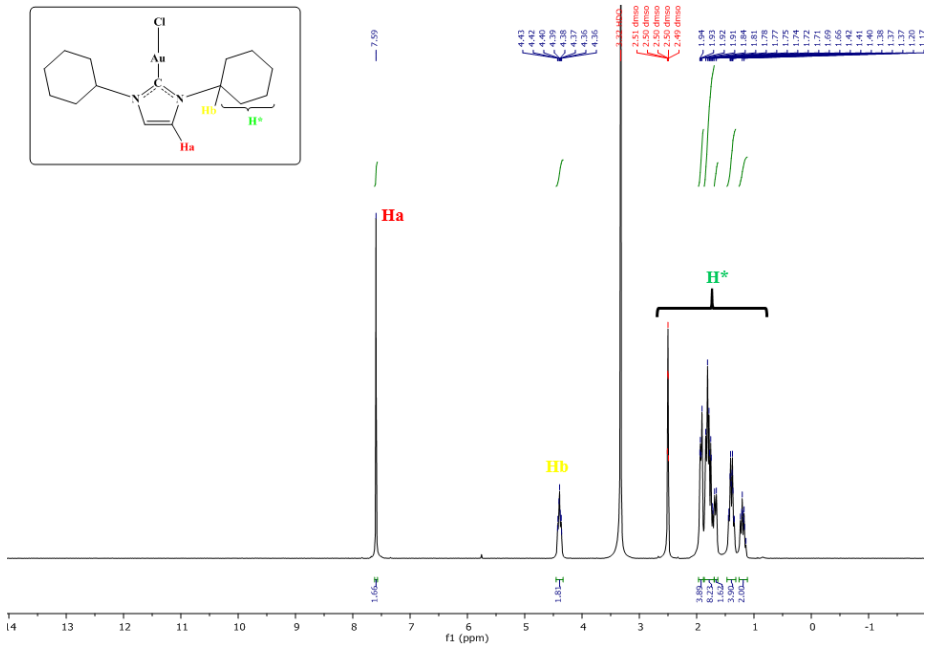

Figure S27. ^{1}H NMR spectrum of complex **4d** (DMSO-d_6, 298K)

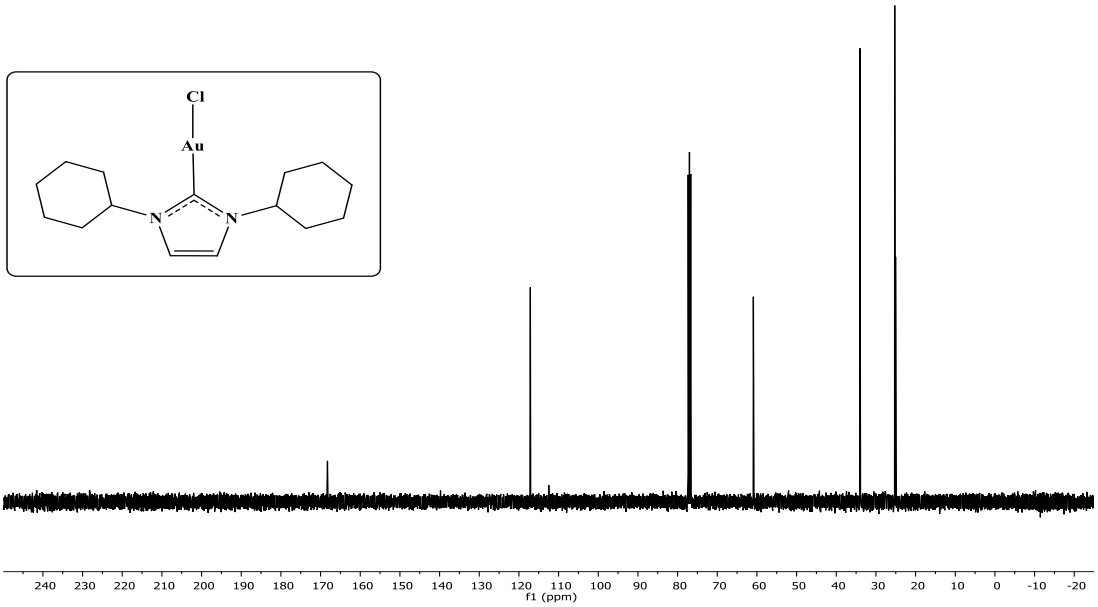

Figure S28. ^{13}C{^{1}H} NMR spectrum of complex **4d** ($CDCl_3$, 298K)

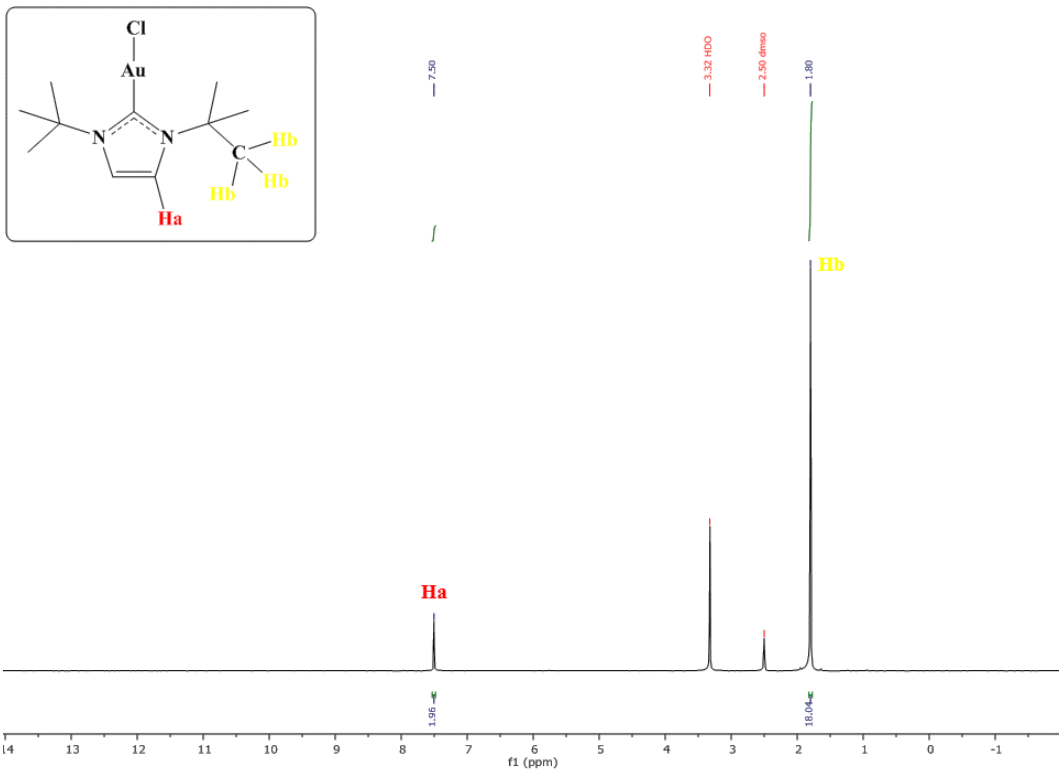

Figure S29. ^{1}H NMR spectrum of complex **4e** (DMSO-d_6, 298K)

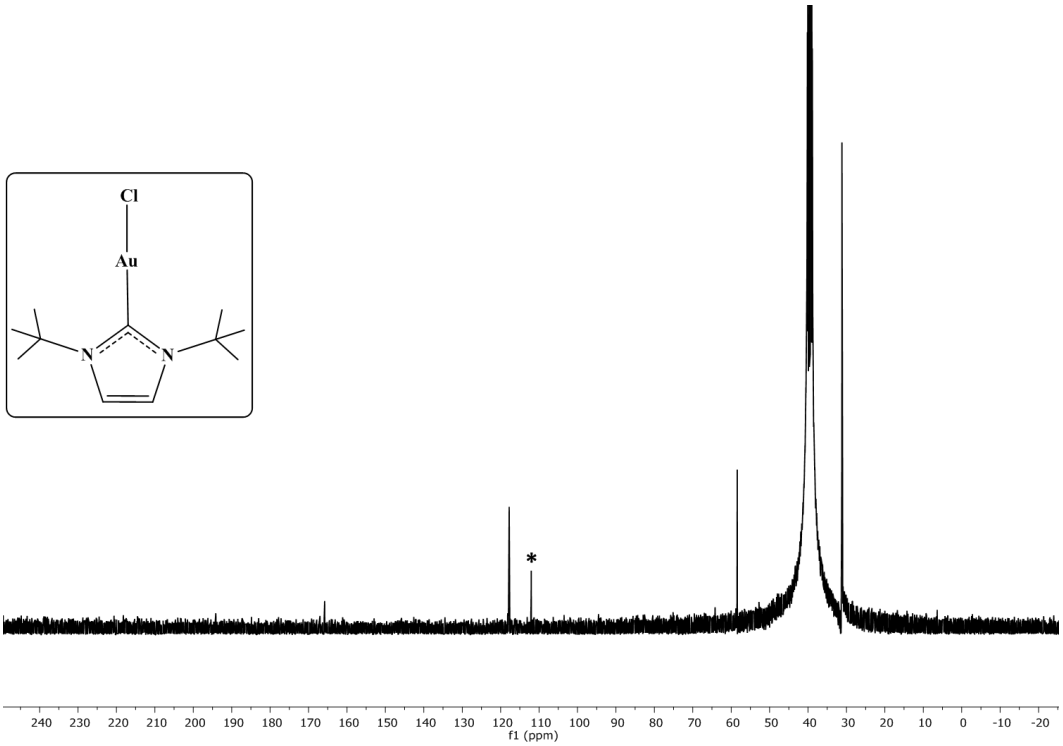

Figure S30. ^{13}C{^{1}H} NMR spectrum of complex **4e** (DMSO-d_6, 298K), * indicates mechanical noise.

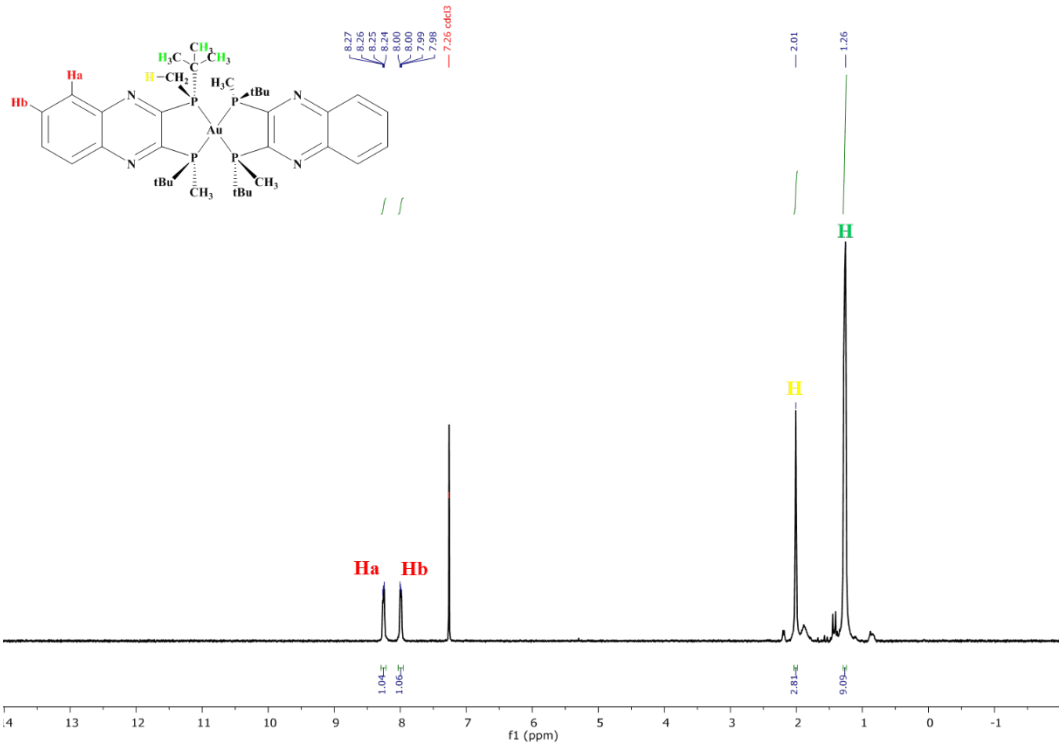

Figure S31. ^{1}H NMR spectrum of Bis(2,3-tert-butylmethylphosphino)quinoxaline)aurate(I) ($CDCl_3$, 298K)

Figure S32. ^{31}P{^{1}H} NMR spectrum of Bis(2,3-tert-butylmethylphosphino)quinoxaline)aurate(I) ($CDCl_3$, 298K). * indicates impurity.

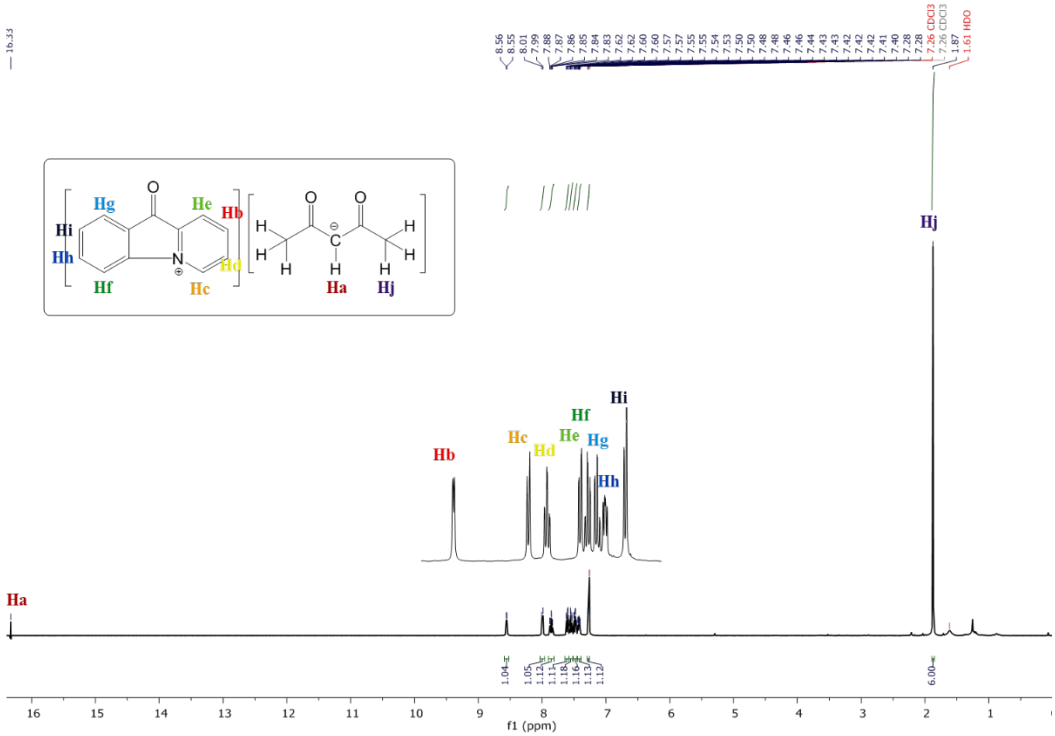

Figure S33. ^{1}H NMR spectrum of 10-oxo-10H-pyrido[1,2-a]indol-5-ium ($CDCl_3$, 298K).

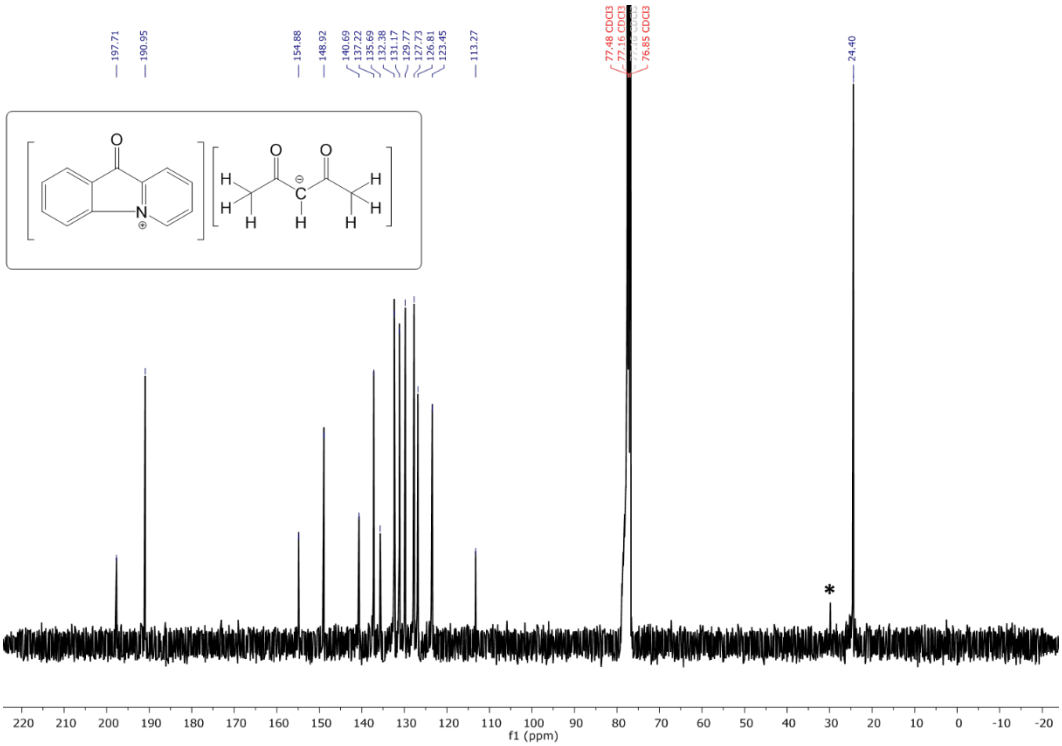

Figure S34. ^{13}C NMR spectrum of 10-oxo-10H-pyrido[1,2-a]indol-5-ium ($CDCl_3$, 298K). * indicates impurities.

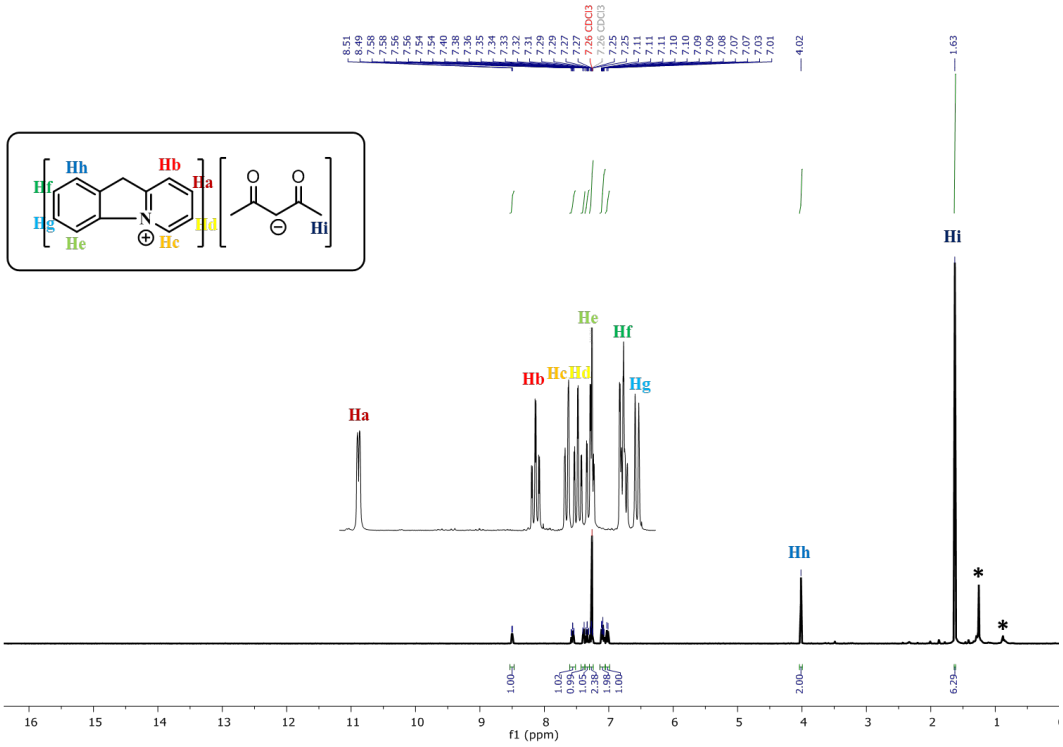

Figure S35. ^{1}H NMR spectrum of 10H-pyrido[1,2-a]indol-5-ium 2,4-dioxopentan-3-ide ($CDCl_3$, 298K). * indicates impurities

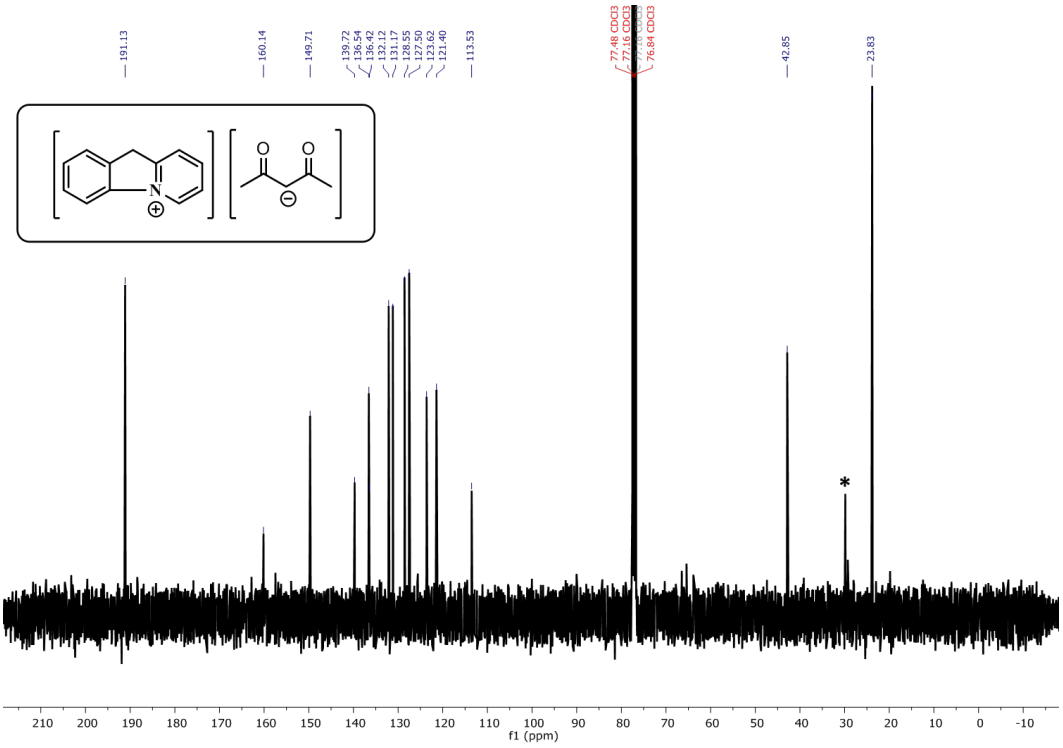

Figure S36. ^{13}C NMR spectrum of 10H-pyrido[1,2-a]indol-5-ium 2,4-dioxopentan-3-ide ($CDCl_3$, 298K). * indicates impurity

X-ray crystallography

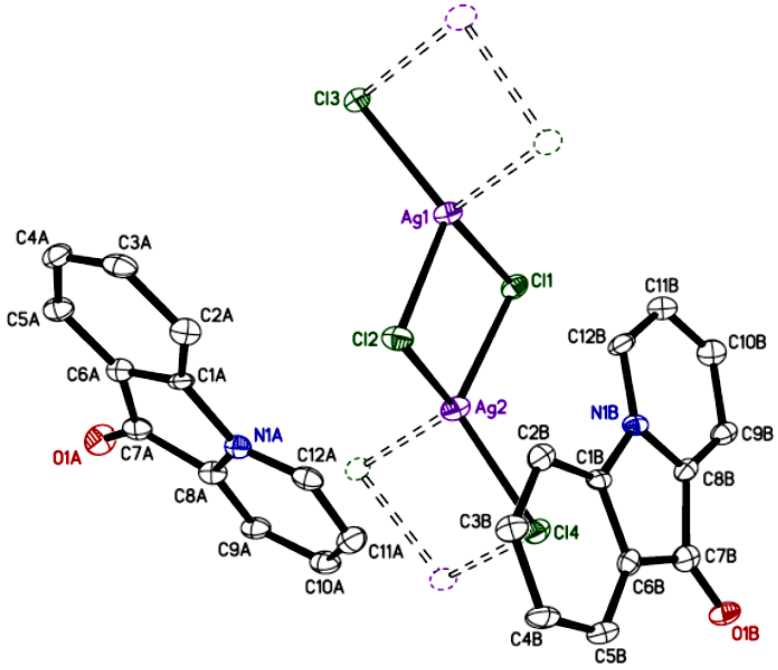

Figure S37. An ellipsoid plot (50% probability) of 2-benzoylpyridium cation (**3**) from the crystal structure. Hydrogen atoms are omitted for clarity.

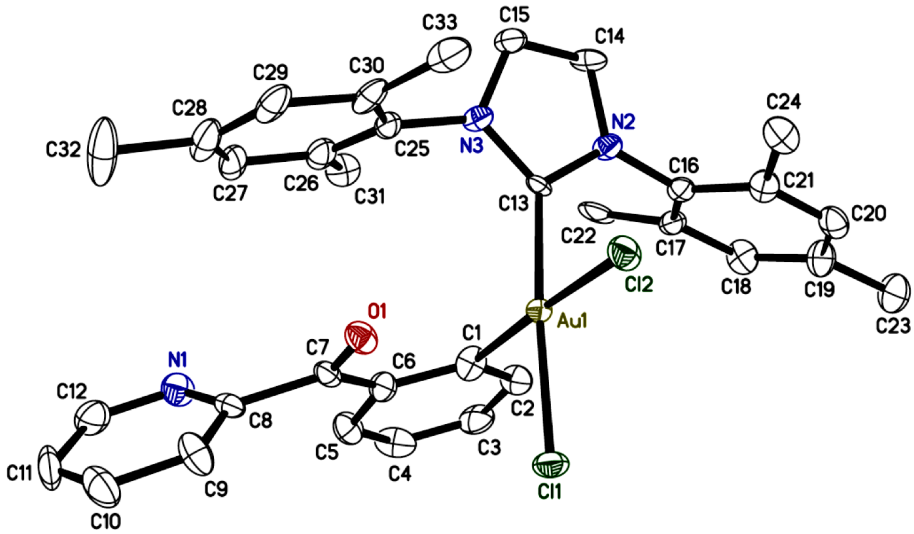

Figure S38. An ellipsoid plot (50% probability) of unconfirmed intermediate from the crystal structure. Hydrogen atoms are omitted for clarity. This is a very similar structure as **IM2** except that two chlorine atoms locate cis position.

Supplementary Figures

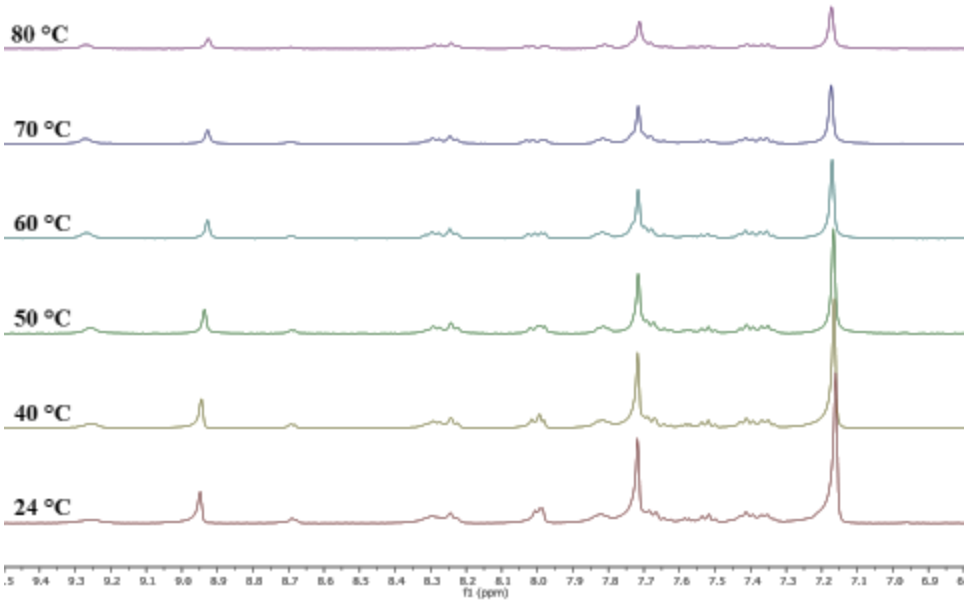

Figure S39. ^{1}H NMR spectra of complex **1** + **2a [IMes.Cl]** mixture (without $NBu_4(acac)$) in CD_3CN at the various temperature.

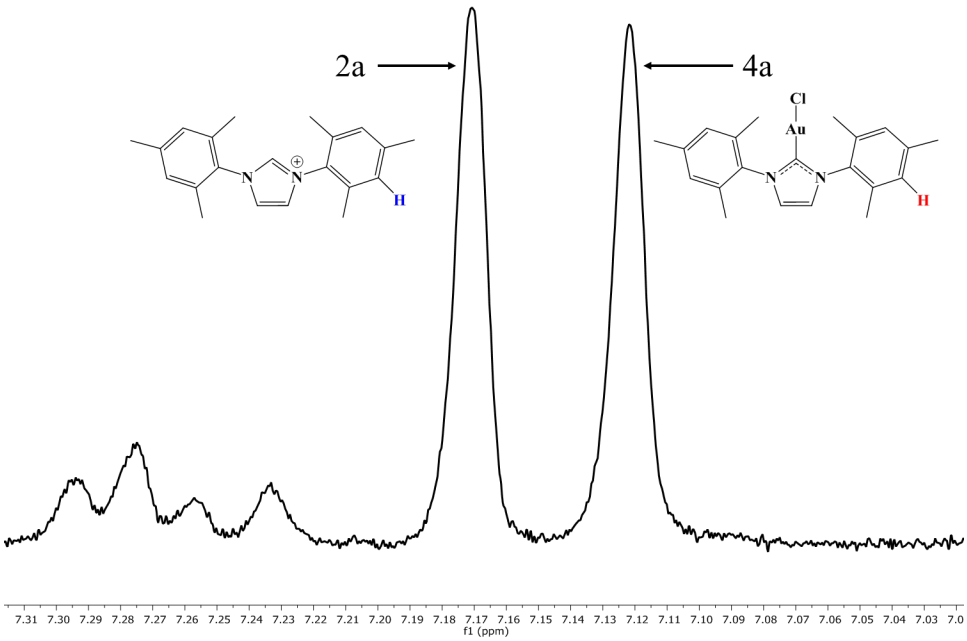

Figure S40. ^{1}H NMR spectrum of the reaction of complex **1** + **2a [IMes.Cl]** with $NBu_4(acac)$ (1.5 equiv) in CD_3CN at 80°C.

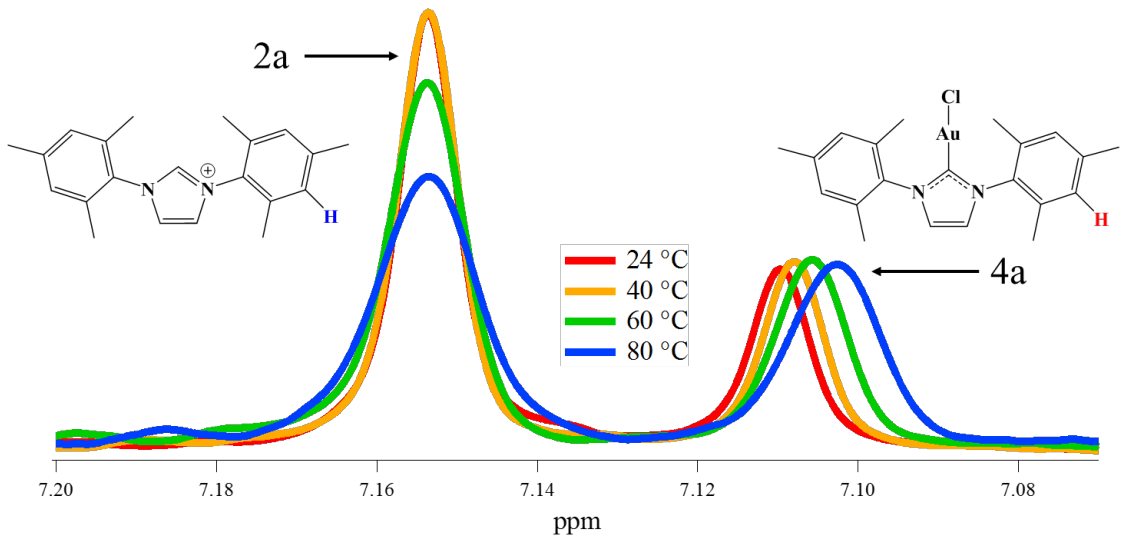

Figure S41. Temperature dependence of ^{1}H NMR spectra of the reaction of complex **1** + **2a [IMes.Cl]** with $NBu_4(acac)$ (1.5 equiv) in CD_3CN.

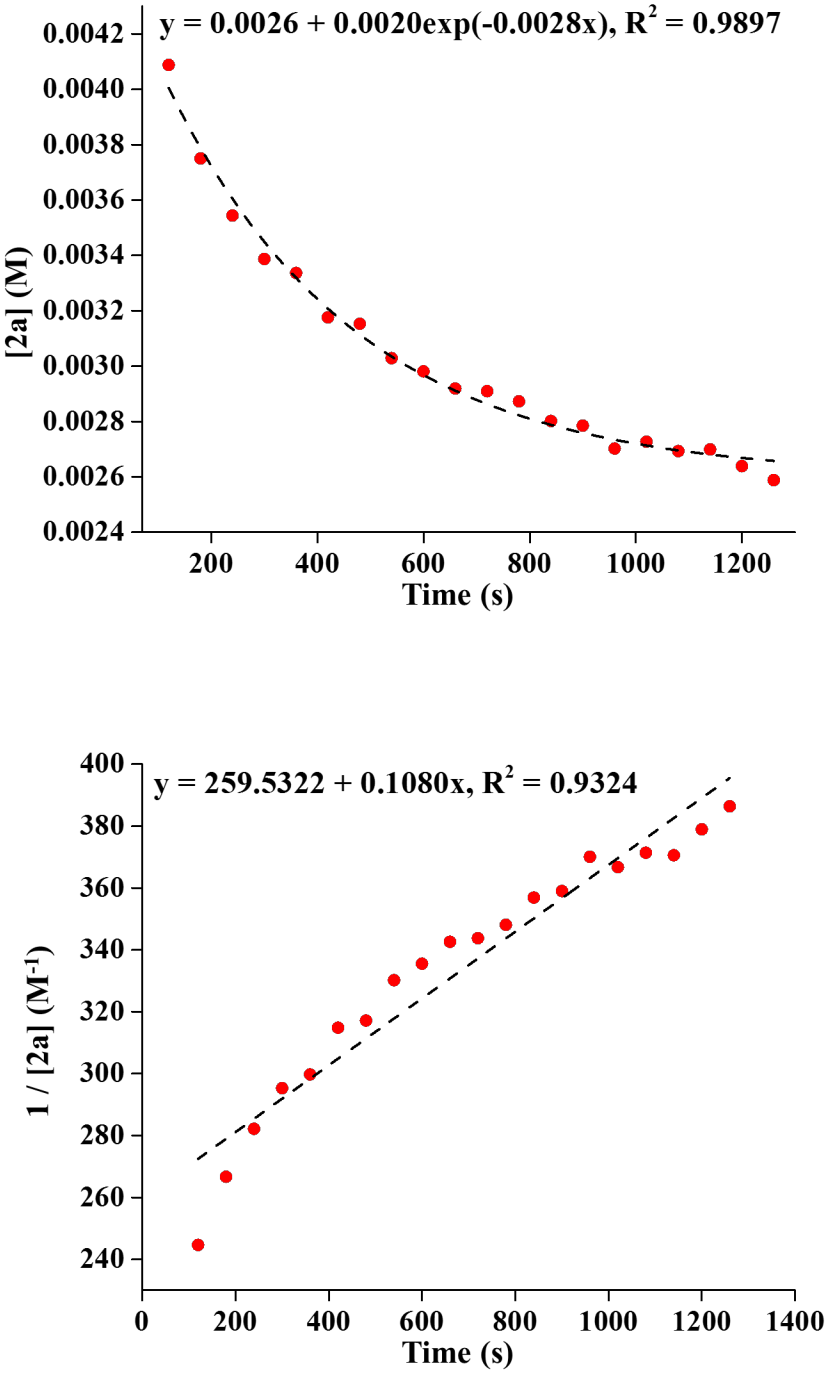

Figure S42. Plots of [**2a**] against time (top) and of 1/[**2a**] against time (bottom) with 1.00 equiv. of $NBu_4(acac)$ at 80 °C in the reaction of **1**+**2a**.

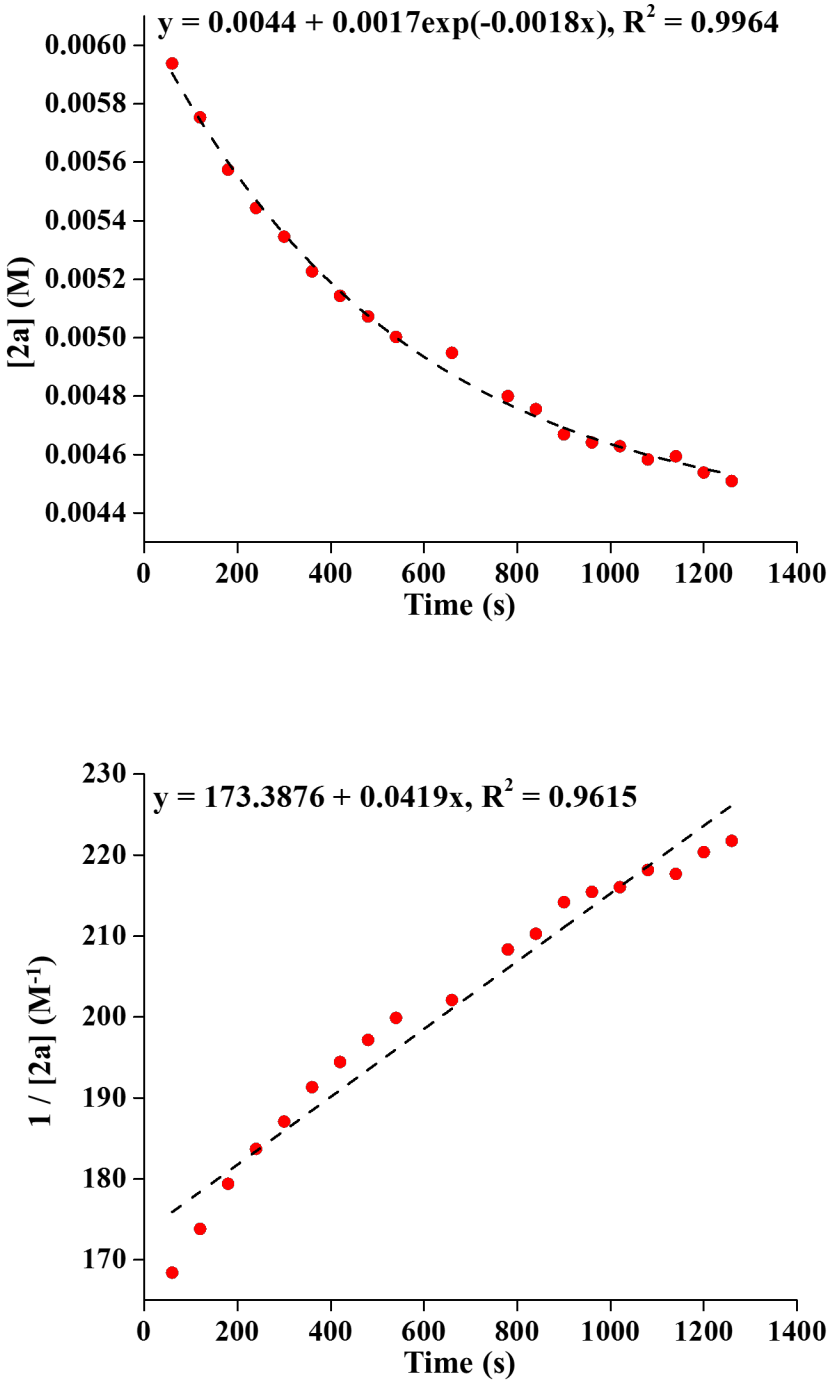

Figure S43. Plots of [**2a**] against time (top) and of 1/[**2a**] against time (bottom) with 1.25 equiv. of $NBu_4(acac)$ at 80 °C in the reaction of **1**+**2a**.

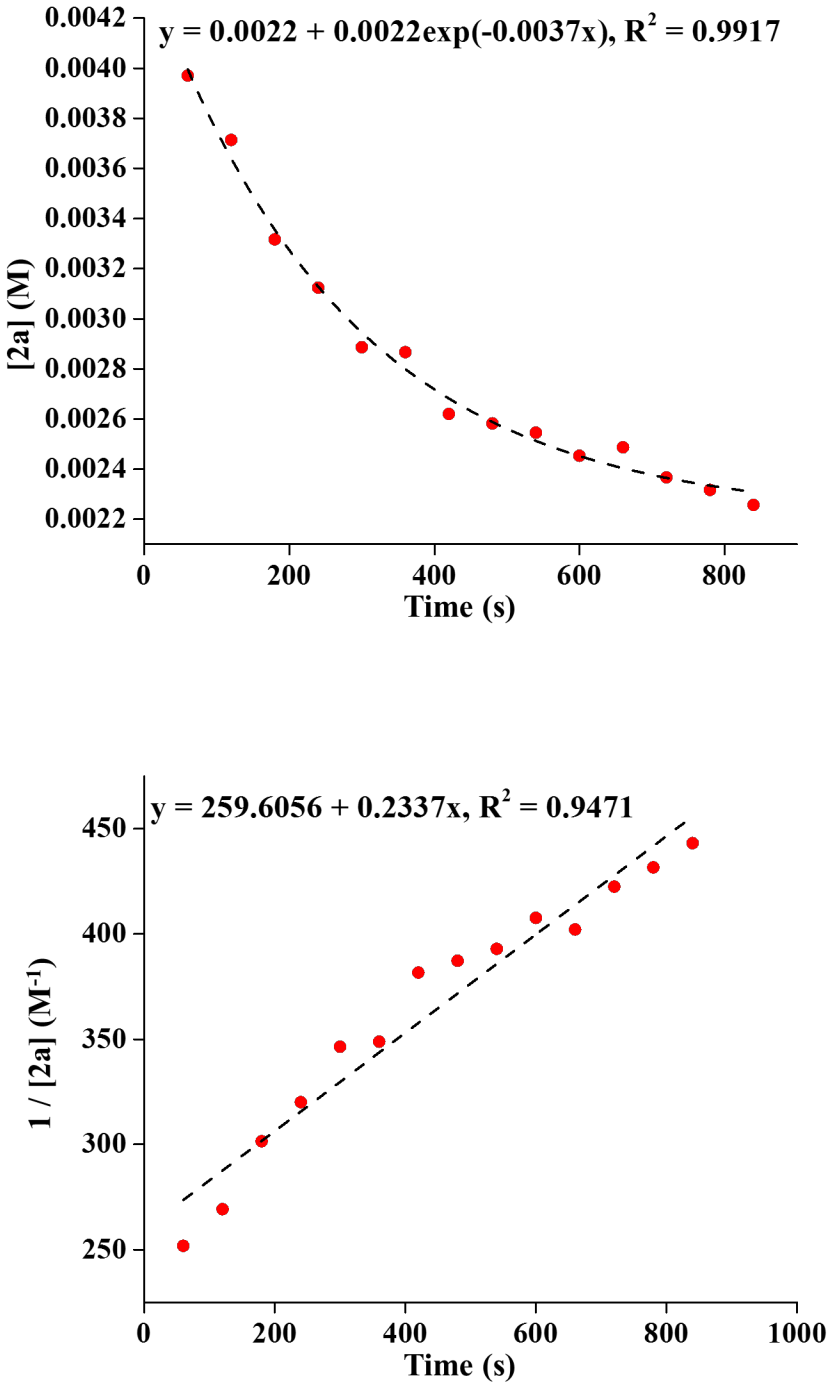

Figure S44. Plots of [**2a**] against time (top) and of 1/[**2a**] against time (bottom) with 1.50 equiv. of $NBu_4(acac)$ at 80 °C in the reaction of **1**+**2a**.

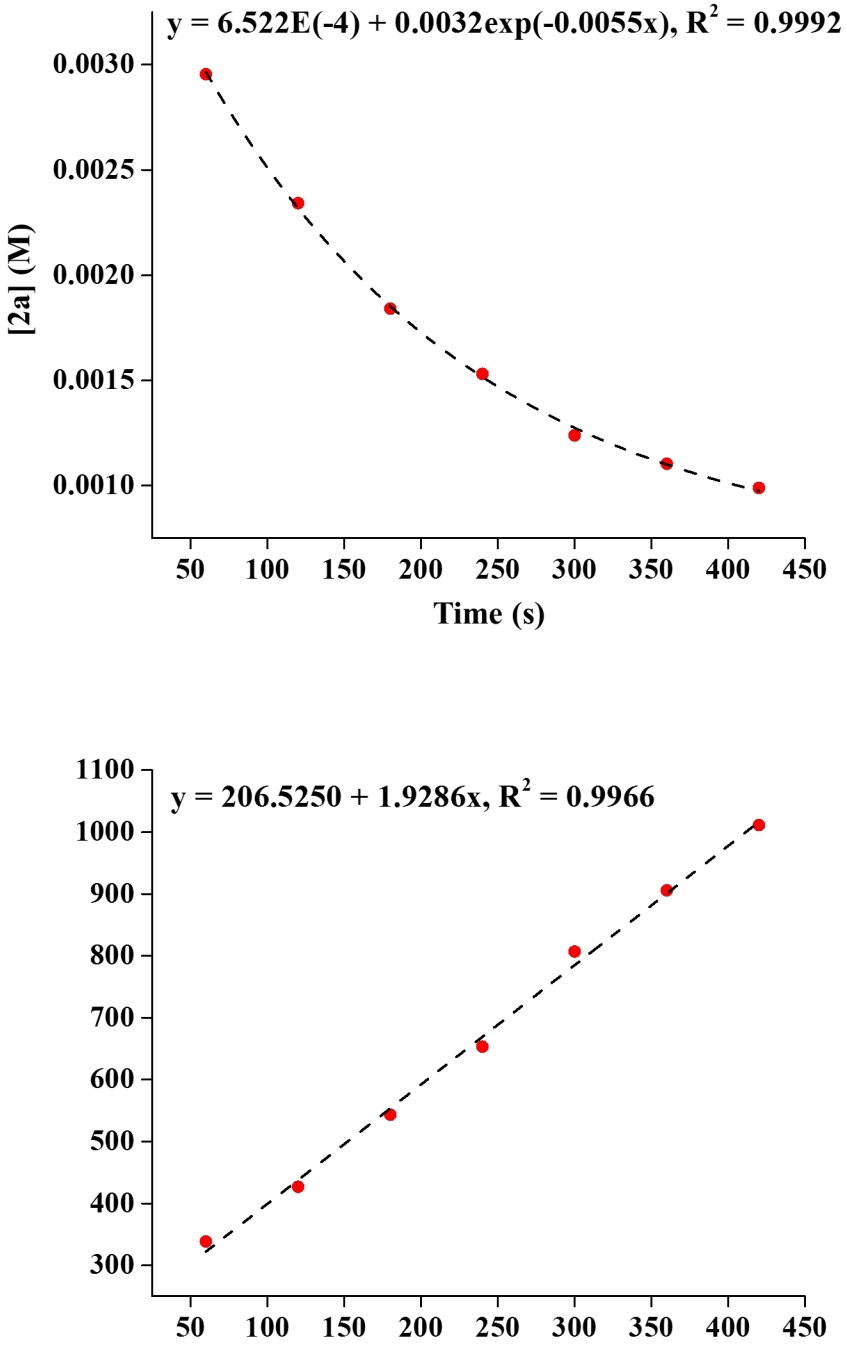

Figure S45. Plots of [**2a**] against time (top) and of 1/[**2a**] against time (bottom) with 1.75 equiv. of $NBu_4(acac)$ at 80 °C in the reaction of **1**+**2a**.

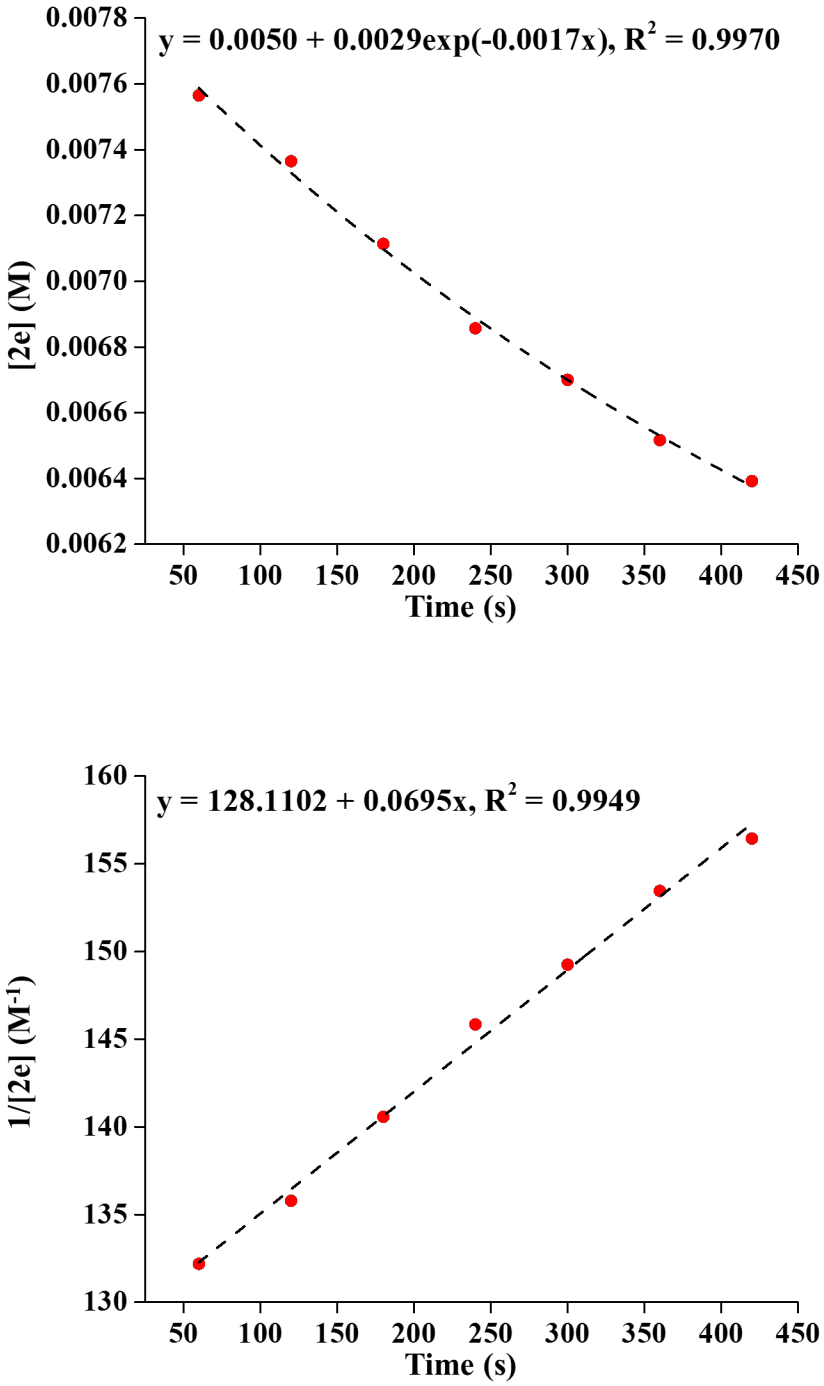

Figure S46. Plots of [**2e**] against time (top) and of 1/[**2e**] against time (bottom) with 1.50 equiv. of $NBu_4(acac)$ at 80 °C in the reaction of **1**+**2e**.

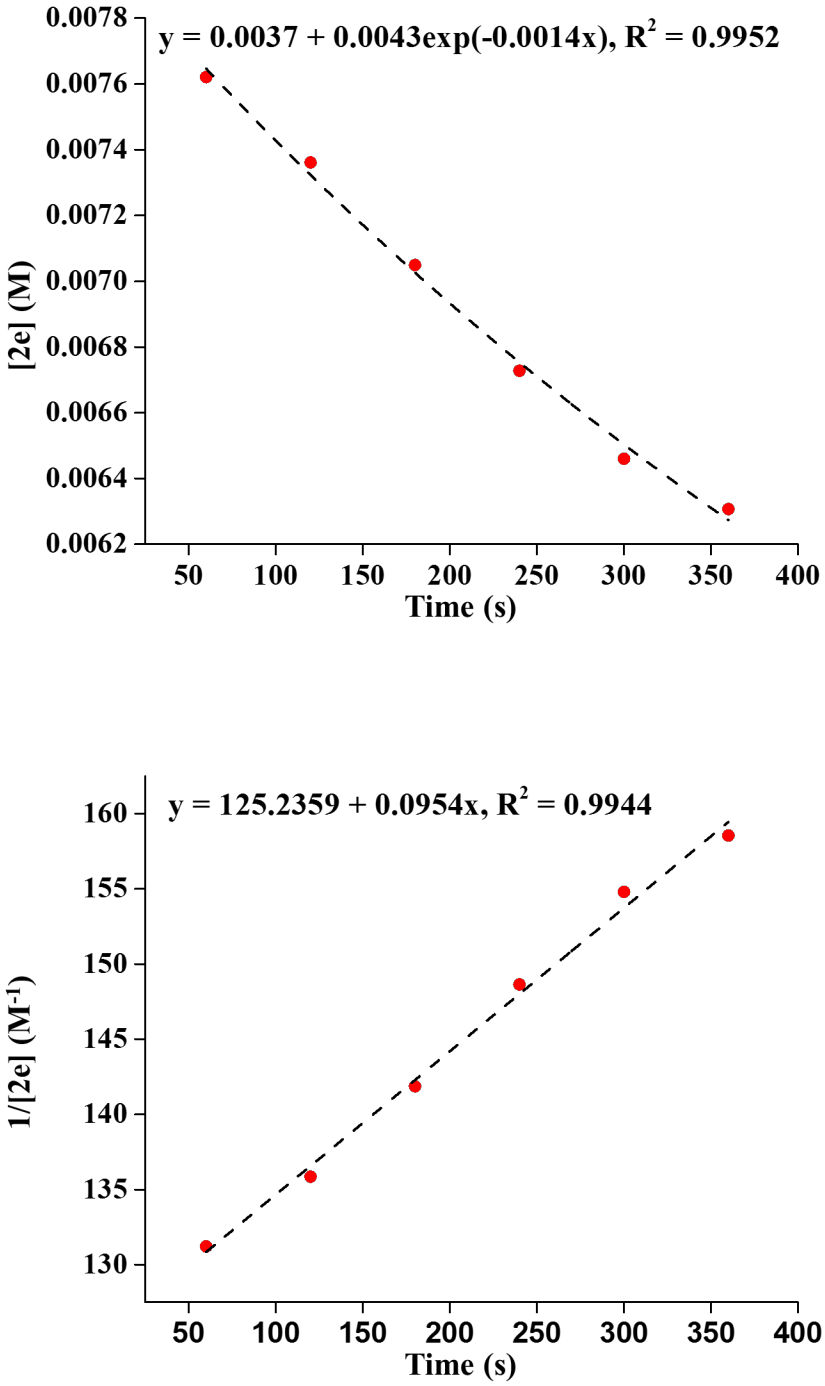

Figure S47. Plots of [**2e**] against time (top) and of 1/[**2e**] against time (bottom) with 1.75 equiv. of $NBu_4(acac)$ at 80 °C in the reaction of **1**+**2e**.

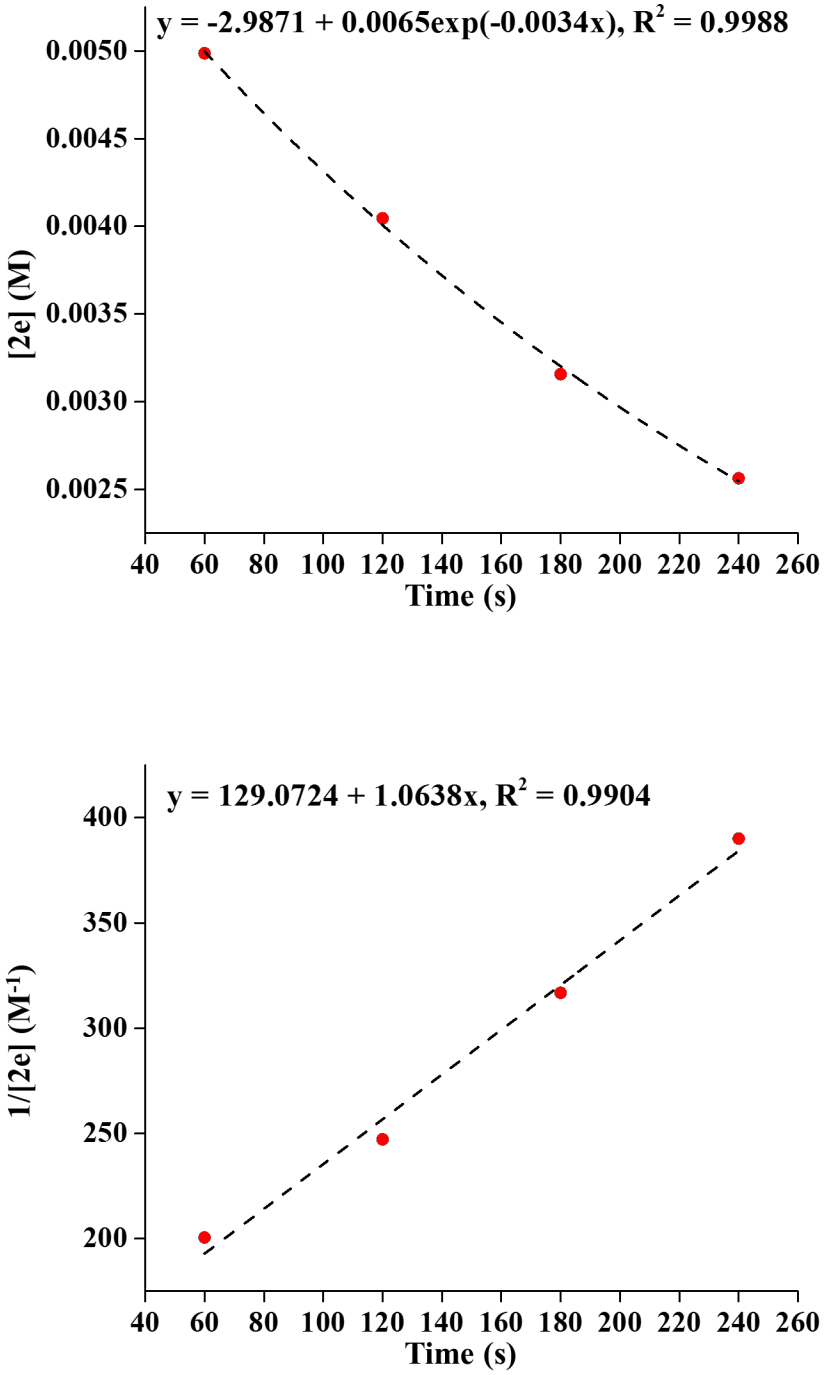

Figure S48. Plots of [**2e**] against time (top) and of 1/[**2e**] against time (bottom) with 2.00 equiv. of $NBu_4(acac)$ at 80 °C in the reaction of **1**+**2e**.

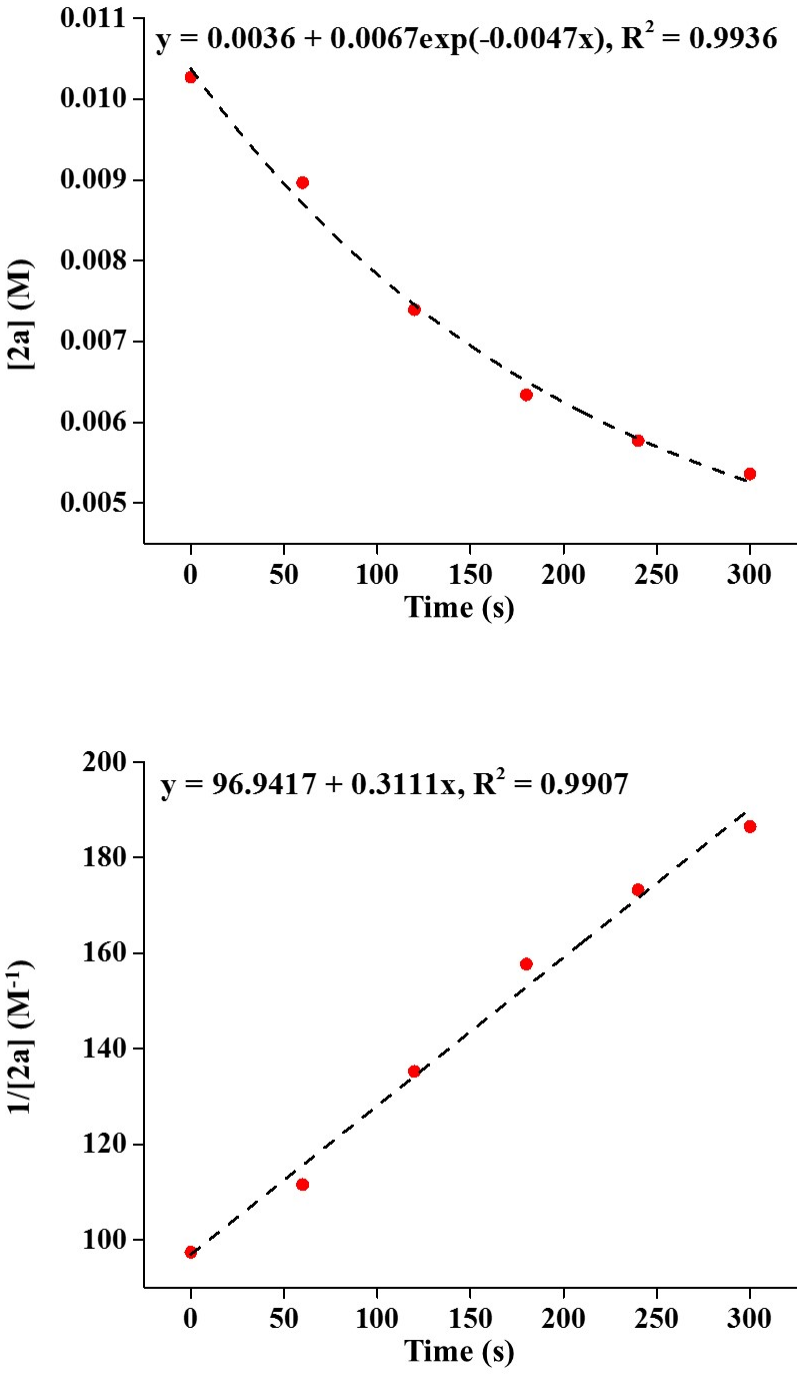

Figure S49. Plots of [**2a**] against time (top) and of 1/[**2a**] against time (bottom) with 1.75 equiv. of $NBu_4(acac)$ at 80 °C in the reaction of **1'**+**2a**.

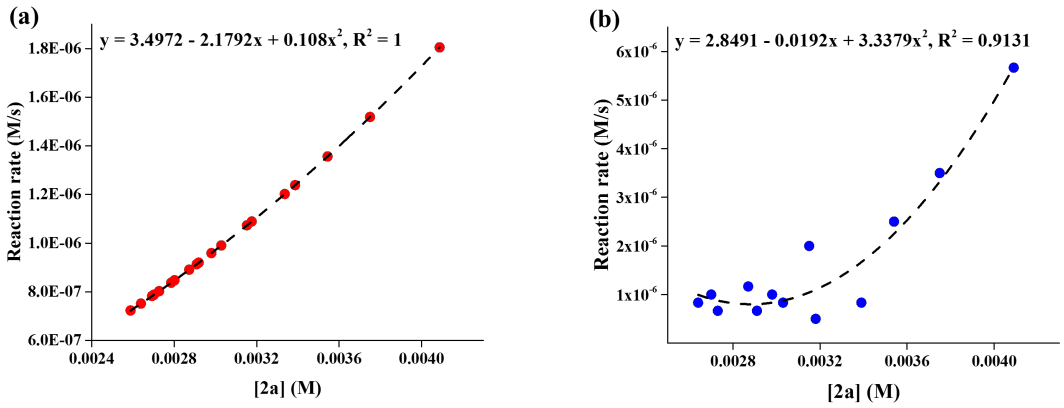

Figure S50. Plot of reaction rate (M/sec) at 80 °C against [**2a**] for the reaction of complex **1** + **2a** with [NBu_4(acac)] = 0.0096 M (1 equiv.). (a) Rate was calculated on the measured *k* (rate const.) and [2a] was measured in proportion to the area of the nmr peak (b) Rate was directly determined by the slope of Figure S42, the plot of change in [2a] over change in time. Both indicate this reaction is 2nd order.

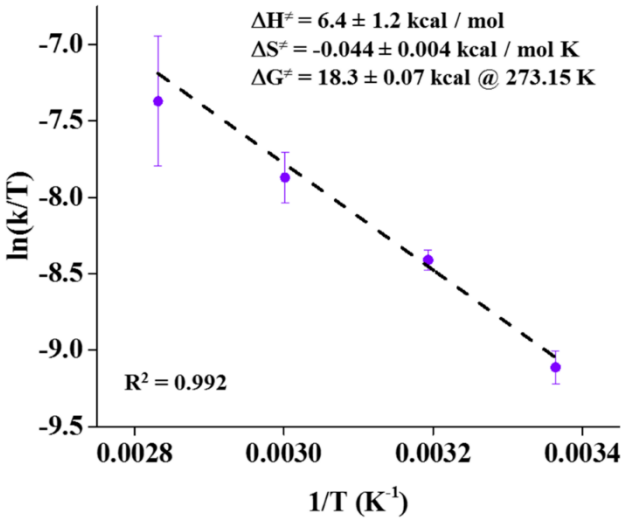

1/Temp (K^{-1})	ln(k/T)
0.0034	-9.11 ± 0.16
0.0032	-8.41 ± 0.08
0.0030	-7.87 ± 0.27
0.0028	-7.37 ± 1.13

Figure S51. Erying plot of the reaction of **1**+ **2a** with 1.75 equiv. of NBu_4(acac) between 24 - 80 °C.

Fukui indices for the metal center.

The Fukui function is defined as:

$$f(\vec{r}) \equiv \left(\frac{\partial \rho_{(\vec{r})}}{\partial N}\right)_{v(\vec{r})} = \left(\frac{\delta \mu}{\delta v(\vec{r})}\right)_{N}$$

With right- and left-hand side derivatives:

$$f^{+}(\vec{r}) = \left(\frac{\partial \rho_{(\vec{r})}}{\partial N}\right)^{+}_{v(\vec{r})}$$

$$f^{-}(\vec{r}) = \left(\frac{\partial \rho_{(\vec{r})}}{\partial N}\right)^{-}_{v(\vec{r})}$$

A site for which the nucleophilic Fukui function $f^{+}(\vec{r})$ has a large value is a site capable of accepting electronic density and a large value of $f^{-}(\vec{r})$ indicates an electron donating site.

Assigning indices to atoms needs the integration of the Fukui around atomic portions of the molecule, leading to condensed to atoms Fukui function (*i.e.* Fukui indices); as done for the condensation of electron density to atoms for determining atomic charges. Therefore, for the atom site *k*, Fukui indices (F^{+} and F^{-}) are defined in terms of atomic populations (p):

$$F_k^{+} = \int \left(\frac{\partial \rho^{k}_{(\vec{r})}}{\partial N}\right)^{+}_{v(\vec{r})} d\vec{r} = \left(\frac{\partial p^{k}}{\partial N}\right)^{+}_{v(\vec{r})} = p^{k}_{N+1} - p^{k}_{N} = q^{k}_{N} - q^{k}_{N+1}$$

$$F_k^{-} = \int \left(\frac{\partial \rho^{k}_{(\vec{r})}}{\partial N}\right)^{-}_{v(\vec{r})} d\vec{r} = \left(\frac{\partial p^{k}}{\partial N}\right)^{-}_{v(\vec{r})} = p^{k}_{N} - p^{k}_{N-1} = q^{k}_{N-1} - q^{k}_{N}$$

For these calculations, as the attributed charge on the metal center is critical, we employed a relativistic approximation instead of the use of an effective core potential. All three population analysis schemes give higher Fukui indices on the metal center for 1 in comparison to the less reactive 1'.

	1		**1'**	
Charges	q_N^{Au}	q_{N+1}^{Au}	q_N^{Au}	q_{N+1}^{Au}
Mulliken	+0.661	+0.619	+0.612	+0.585
Loewdin	-0.478	-0.517	-0.509	-0.540
Hirshfeld	+0.455	+0.421	+0.437	+0.413
F+				
Mulliken	0.041		0.027	
Loewdin	0.040		0.031	
Hirshfeld	0.034		0.025	

Figure S52. Fukui indices for the metal center.

Proposed stepwise mechanism:

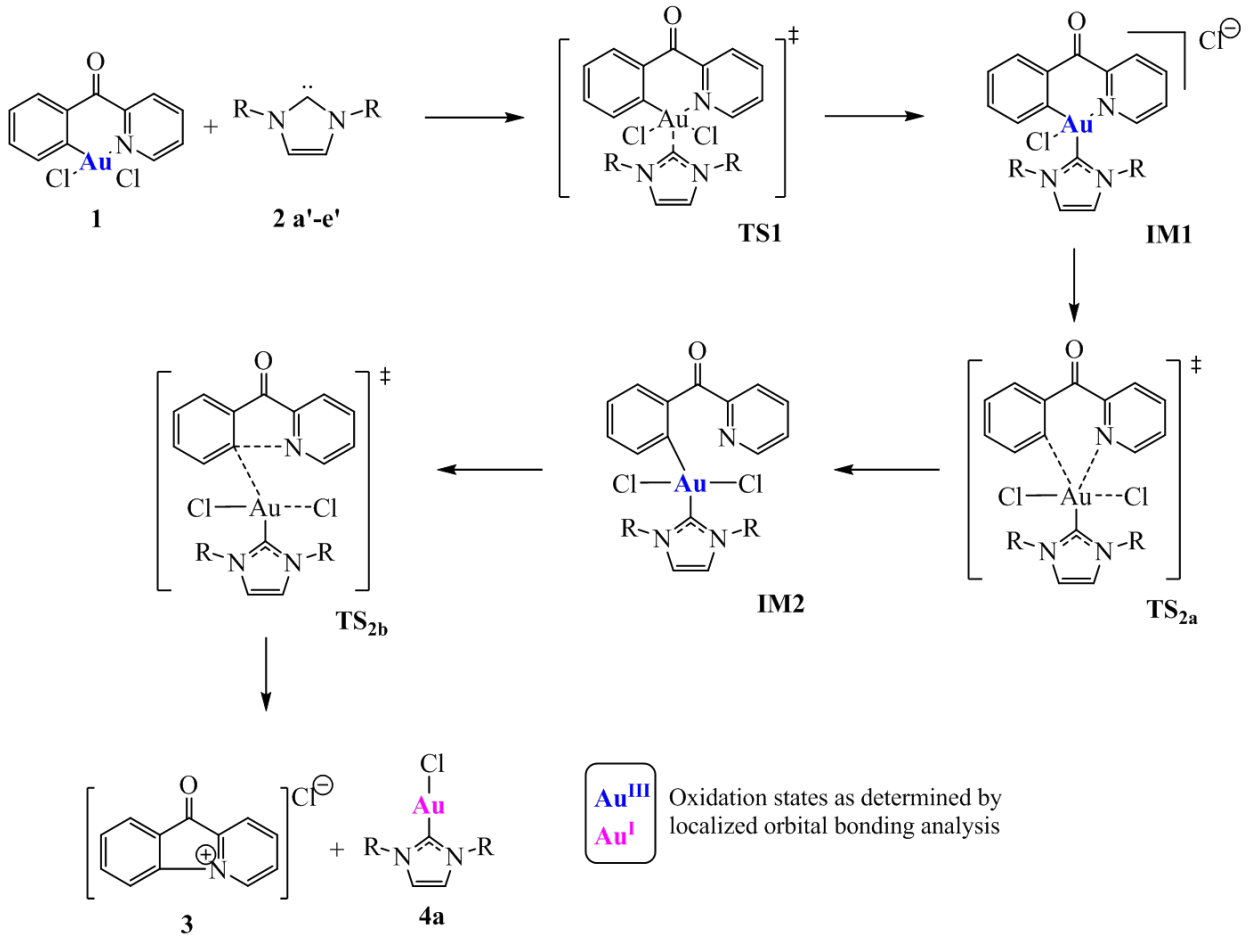

Figure S53. Proposed mechanism of the reaction of complex **1** with **2a**. **2a'** indicates the **2a**-generated carbene by reaction with $NBu_4(acac)$.

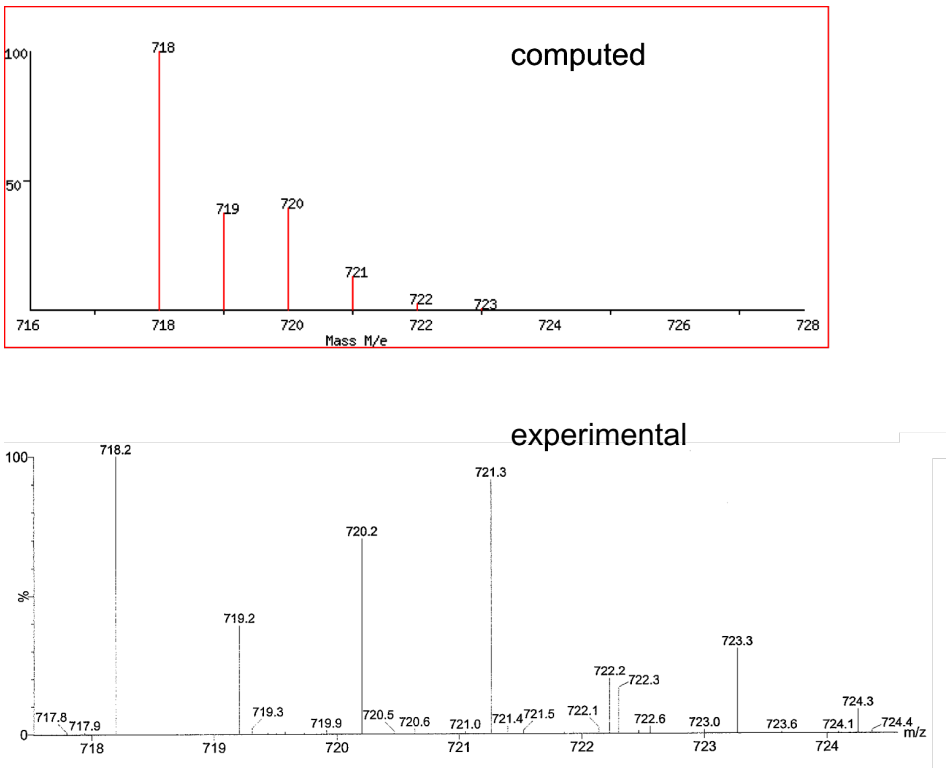

Figure S54. LR-MS spectrum of IM1 (m/z=718.2), computed (above) and measured (below). ESI, positive ion mode, and TOF MS were used.

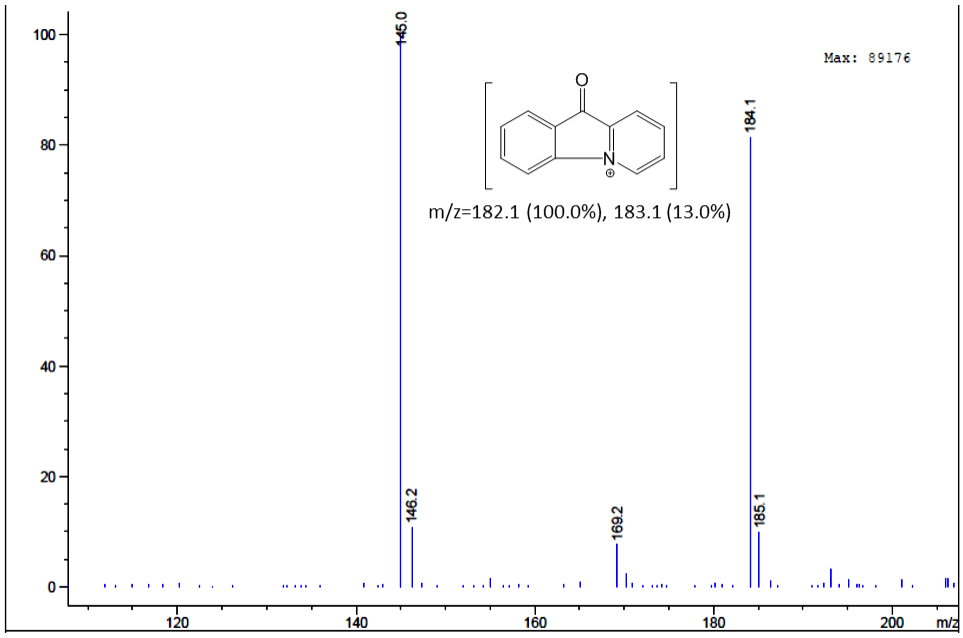

Figure S55. LR-MS spectrum of 3 ($[M+2H]^+$, m/z=184.1). ES-API and positive ion mode were used.

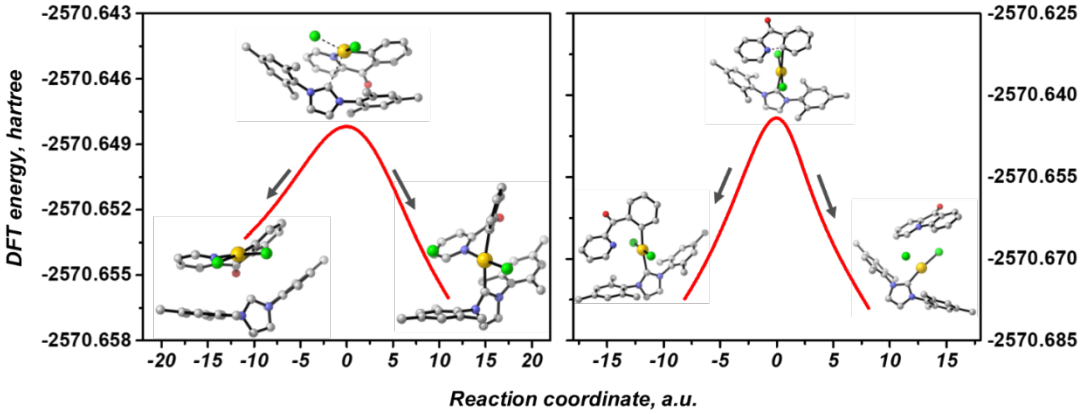

Figure S56. Intrinsic reaction coordinate pathways for TS1 and TS2 (ωB97x-D/def2-SVP).

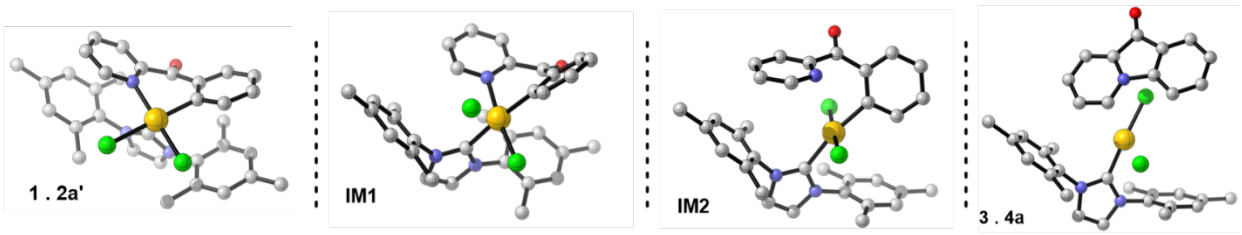

Figure S57. Calculated equilibrium geometries along the reaction path (ωB97x-D/def2-TZVP//MeCN). All complexes except for the final products involve Au(III) species; the final complex being an Au(I) species (all oxidation states were confirmed by LOBA, see computational details).

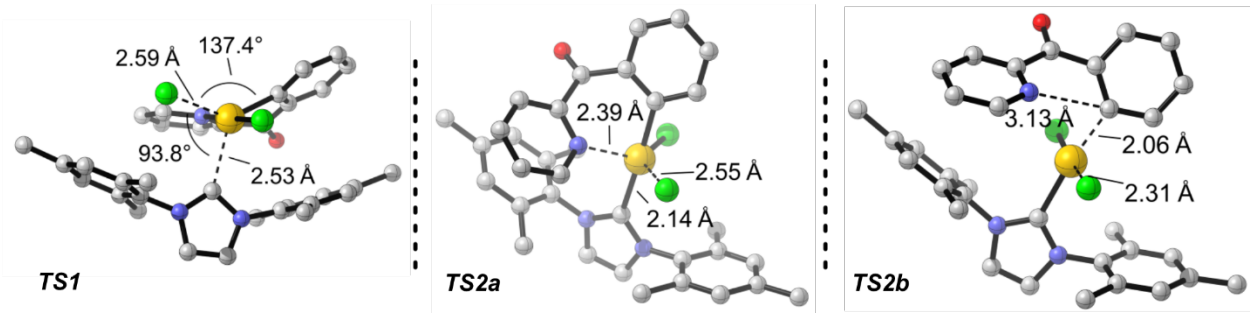

Figure S58. Calculated transition state structures along the reaction path (ωB97x-D/def2-TZVP//MeCN).

Supporting Tables

Table S1. Crystal data and structure refinement for compound **3**.

Empirical formula	C24 H16 Ag2 Cl4 N2 O2
Formula weight	721.93
Temperature	90.0(2) K
Wavelength	0.71073 Å
Crystal system, space group	Monoclinic, $P2_1/n$
Unit cell dimensions	a = 6.8483(2) Å alpha = 90 deg.
	b = 14.6095(5) Å beta = 97.371(2) deg.
	c = 23.8424(10) Å gamma = 90 deg.
Volume	2365.73(15) $Å^3$
Z, Calculated density	4, 2.027 Mg/m^3
Absorption coefficient	2.134 mm^{-1}
F(000)	1408
Crystal size	0.240 x 0.200 x 0.140 mm
Theta range for data collection	2.216 to 27.468 deg.
Limiting indices	-8<=h<=8, -17<=k<=18, -30<=l<=30
Reflections collected / unique	17897 / 5285 [R(int) = 0.0467]
Completeness to theta = 25.242	99.1 %
Absorption correction	Semi-empirical from equivalents
Max. and min. transmission	0.746 and 0.607
Refinement method	Full-matrix least-squares on F^2
Data / restraints / parameters	5285 / 0 / 307
Goodness-of-fit on F^2	1.079
Final R indices [I>2sigma(I)]	R1 = 0.0430, wR2 = 0.0661
R indices (all data)	R1 = 0.0805, wR2 = 0.0747
Extinction coefficient	n/a
Largest diff. peak and hole	0.541 and -0.981 e. $Å^{-3}$

Table S2. Crystal data and structure refinement for compound IM2

Empirical formula	C33.77 H33.53 Au Cl3.53 N3 O
Formula weight	819.59
Temperature	90.0(2) K
Wavelength	0.71073 Å
Crystal system, space group	Orthorhombic, $P2_12_12_1$
Unit cell dimensions	a = 11.3471(3) Å alpha = 90 deg.
	b = 13.4416(5) Å beta = 90 deg.
	c = 21.6337(8) Å gamma = 90 deg.
Volume	3299.64(19) $Å^3$
Z, Calculated density	4, 1.650 Mg/m^3
Absorption coefficient	4.776 mm^{-1}
F(000)	1617
Crystal size	0.250 x 0.250 x 0.090 mm
Theta range for data collection	3.011 to 27.501 deg.
Limiting indices	-14<=h<=14, -17<=k<=17, -28<=l<=28
Reflections collected / unique	55092 / 7534 [R(int) = 0.0502]
Completeness to theta = 25.242	99.6 %
Absorption correction	Semi-empirical from equivalents
Max. and min. transmission	0.563 and 0.366
Refinement method	Full-matrix least-squares on F^2
Data / restraints / parameters	7534 / 0 / 397
Goodness-of-fit on F^2	1.208
Final R indices [I>2sigma(I)]	R1 = 0.0379, wR2 = 0.0916
R indices (all data)	R1 = 0.0413, wR2 = 0.0928
Extinction coefficient	0.00124(18)
Largest diff. peak and hole	1.880 and -2.501 $e.A^{-3}$

Table S3. Bond lengths [Å] and angles [deg] for compound **3**.

Bond	Lengths		Bond	Lengths
Ag1-Cl3	2.5322(12)		C2B-H2B	0.95
Ag1-Cl1	2.5370(11)		C3B-C4B	1.396(6)
Ag1-Cl2	2.6140(12)		C3B-H3B	0.95
Ag1-Cl4#1	2.6411(12)		C4B-C5B	1.382(6)
Ag2-Cl4	2.5602(12)		C4B-H4B	0.95
Ag2-Cl2	2.5906(12)		C5B-C6B	1.385(6)
Ag2-Cl1	2.6294(12)		C5B-H5B	0.95
Ag2-Cl3#2	2.6828(12)		C6B-C7B	1.474(6)
O1A-C7A	1.216(5)		C7B-C8B	1.495(6)
N1A-C12A	1.335(5)		C8B-C9B	1.362(6)
N1A-C8A	1.371(5)		C9B-C10B	1.396(6)
N1A-C1A	1.446(5)		C9B-H9B	0.95
C1A-C2A	1.366(6)		C10B-C11B	1.377(6)
C1A-C6A	1.389(6)		C10B-H10B	0.95
C2A-C3A	1.395(6)		C11B-C12B	1.393(6)
C2A-H2A	0.95		C11B-H11B	0.95
C3A-C4A	1.399(6)		C12B-H12B	0.95
C3A-H3A	0.95			
C4A-C5A	1.383(6)			
C4A-H4A	0.95			
C5A-C6A	1.383(6)			
C5A-H5A	0.95			
C6A-C7A	1.485(6)			
C7A-C8A	1.491(6)			
C8A-C9A	1.358(6)			
C9A-C10A	1.396(6)			
C9A-H9A	0.95			
C10A-C11A	1.379(6)			
C10A-H10A	0.95			
C11A-C12A	1.396(6)			
C11A-H11A	0.95			
C12A-H12A	0.95			
O1B-C7B	1.211(5)			
N1B-C12B	1.339(5)			
N1B-C8B	1.376(5)			
N1B-C1B	1.453(5)			
C1B-C2B	1.371(6)			
C1B-C6B	1.386(6)			
C2B-C3B	1.401(6)			

Bond	Angles	Bond	Angles	Bond	Angles
Cl3-Ag1-Cl1	125.53(3)	C6A-C7A-C8A	104.8(4)	C6B-C7B-C8B	105.3(4)
Cl3-Ag1-Cl2	119.54(4)	C9A-C8A-N1A	120.4(4)	C9B-C8B-N1B	120.6(4)
Cl1-Ag1-Cl2	96.92(4)	C9A-C8A-C7A	131.6(4)	C9B-C8B-C7B	131.9(4)
Cl3-Ag1-Cl4#1	98.29(4)	N1A-C8A-C7A	108.0(4)	N1B-C8B-C7B	107.5(4)
Cl1-Ag1-Cl4#1	114.16(4)	C8A-C9A-C10A	119.3(4)	C8B-C9B-C10B	118.0(4)
Cl2-Ag1-Cl4#1	100.55(4)	C8A-C9A-H9A	120.3	C8B-C9B-H9B	121
Cl4-Ag2-Cl2	116.71(4)	C10A-C9A-H9A	120.3	C10B-C9B-H9B	121
Cl4-Ag2-Cl1	121.31(4)	C11A-C10A-C9A	119.0(4)	C11B-C10B-C9B	120.7(4)
Cl2-Ag2-Cl1	95.22(4)	C11A-C10A-H10A	120.5	C11B-C10B-H10B	119.6
Cl4-Ag2-Cl3#2	96.54(4)	C9A-C10A-H10A	120.5	C9B-C10B-H10B	119.6
Cl2-Ag2-Cl3#2	116.66(4)	C10A-C11A-C12A	120.8(4)	C10B-C11B-C12B	119.9(4)
Cl1-Ag2-Cl3#2	111.86(3)	C10A-C11A-H11A	119.6	C10B-C11B-H11B	120
Ag1-Cl1-Ag2	83.92(3)	C12A-C11A-H11A	119.6	C12B-C11B-H11B	120
Ag2-Cl2-Ag1	83.18(3)	N1A-C12A-C11A	118.3(4)	N1B-C12B-C11B	118.4(4)
Ag1-Cl3-Ag2#1	82.14(3)	N1A-C12A-H12A	120.9	N1B-C12B-H12B	120.8
Ag2-Cl4-Ag1#2	82.45(3)	C11A-C12A-H12A	120.9	C11B-C12B-H12B	120.8
C12A-N1A-C8A	122.2(4)	C12B-N1B-C8B	122.3(4)		
C12A-N1A-C1A	127.6(4)	C12B-N1B-C1B	127.5(4)		
C8A-N1A-C1A	110.1(4)	C8B-N1B-C1B	110.1(3)		
C2A-C1A-C6A	123.3(4)	C2B-C1B-C6B	124.0(4)		
C2A-C1A-N1A	128.2(4)	C2B-C1B-N1B	127.8(4)		
C6A-C1A-N1A	108.5(4)	C6B-C1B-N1B	108.3(4)		
C1A-C2A-C3A	116.5(4)	C1B-C2B-C3B	115.6(4)		
C1A-C2A-H2A	121.8	C1B-C2B-H2B	122.2		
C3A-C2A-H2A	121.8	C3B-C2B-H2B	122.2		
C2A-C3A-C4A	121.3(4)	C4B-C3B-C2B	121.7(4)		
C2A-C3A-H3A	119.3	C4B-C3B-H3B	119.2		
C4A-C3A-H3A	119.3	C2B-C3B-H3B	119.2		
C5A-C4A-C3A	120.6(4)	C5B-C4B-C3B	120.6(4)		
C5A-C4A-H4A	119.7	C5B-C4B-H4B	119.7		
C3A-C4A-H4A	119.7	C3B-C4B-H4B	119.7		
C6A-C5A-C4A	118.3(4)	C4B-C5B-C6B	118.5(4)		
C6A-C5A-H5A	120.8	C4B-C5B-H5B	120.8		
C4A-C5A-H5A	120.8	C6B-C5B-H5B	120.8		
C5A-C6A-C1A	119.9(4)	C5B-C6B-C1B	119.6(4)		
C5A-C6A-C7A	131.7(4)	C5B-C6B-C7B	131.6(4)		
C1A-C6A-C7A	108.4(4)	C1B-C6B-C7B	108.8(4)		
O1A-C7A-C6A	129.5(4)	O1B-C7B-C6B	129.1(4)		
O1A-C7A-C8A	125.7(4)	O1B-C7B-C8B	125.6(4)		

Table S4. Bond lengths [Å] and angles [deg] for calculated complex **IM1**.

Atom label	Lengths		Atom label	Lengths
R(1,2)	1.4029		R(33,35)	1.3988
R(1,6)	1.3911		R(33,52)	1.5102
R(1,22)	2.0524		R(34,36)	1.3996
R(2,3)	1.407		R(34,48)	1.5093
R(2,11)	1.4922		R(35,37)	1.3996
R(3,4)	1.3915		R(35,38)	1.0868
R(3,7)	1.0851		R(36,37)	1.399
R(4,5)	1.396		R(36,39)	1.0868
R(4,8)	1.0851		R(37,56)	1.5096
R(5,6)	1.4009		R(40,41)	1.4062
R(5,9)	1.0857		R(40,42)	1.4086
R(6,10)	1.0815		R(41,43)	1.3991
R(11,12)	1.2217		R(41,60)	1.5076
R(11,13)	1.5128		R(42,44)	1.3994
R(13,14)	1.392		R(42,64)	1.5128
R(13,23)	1.353		R(43,45)	1.3989
R(14,16)	1.3951		R(43,46)	1.0866
R(14,17)	1.0829		R(44,45)	1.3983
R(15,18)	1.3938		R(44,47)	1.0869
R(15,19)	1.0877		R(45,68)	1.5094
R(15,23)	1.3458		R(48,49)	1.0964
R(16,18)	1.3916		R(48,50)	1.0918
R(16,20)	1.0848		R(48,51)	1.0924
R(18,21)	1.0837		R(52,53)	1.0918
R(19,72)	2.5152		R(52,54)	1.0962
R(22,23)	2.1186		R(52,55)	1.0919
R(22,24)	2.4574		R(56,57)	1.0935
R(22,25)	2.0628		R(56,58)	1.0968
R(25,30)	1.3596		R(56,59)	1.0937
R(25,31)	1.3604		R(60,61)	1.0953
R(26,27)	1.3538		R(60,62)	1.0922
R(26,28)	1.0777		R(60,63)	1.0922
R(26,30)	1.3887		R(64,65)	1.0926
R(27,29)	1.0775		R(64,66)	1.0965
R(27,31)	1.3913		R(64,67)	1.0914
R(30,32)	1.4508		R(68,69)	1.0968
R(31,40)	1.4522		R(68,70)	1.0938
R(32,33)	1.407		R(68,71)	1.0935
R(32,34)	1.4059			

Atom label	Angles		Atom label	Angles		Atom label	Angles
A(2,1,6)	120.3026		A(23,22,24)	87.7748		A(31,40,42)	117.9354
A(2,1,22)	116.3765		A(24,22,25)	91.7461		A(41,40,42)	122.1039
A(6,1,22)	123.2859		A(13,23,15)	120.4724		A(40,41,43)	117.4583
A(1,2,3)	119.2774		A(13,23,22)	117.8787		A(40,41,60)	122.4306
A(1,2,11)	124.1933		A(15,23,22)	120.3341		A(43,41,60)	120.0426
A(3,2,11)	116.2423		A(22,25,30)	123.1853		A(40,42,44)	117.6024
A(2,3,4)	120.431		A(22,25,31)	130.6324		A(40,42,64)	122.9338
A(2,3,7)	118.4459		A(30,25,31)	105.9482		A(44,42,64)	119.3562
A(4,3,7)	121.0881		A(27,26,28)	131.4315		A(41,43,45)	122.2574
A(3,4,5)	119.631		A(27,26,30)	106.9698		A(41,43,46)	118.4007
A(3,4,8)	120.0216		A(28,26,30)	121.5973		A(45,43,46)	119.3331
A(5,4,8)	120.3351		A(26,27,29)	131.3896		A(42,44,45)	122.0511
A(4,5,6)	120.4495		A(26,27,31)	107.2399		A(42,44,47)	118.52
A(4,5,9)	120.2672		A(29,27,31)	121.37		A(45,44,47)	119.4208
A(6,5,9)	119.2795		A(25,30,26)	110.0801		A(43,45,44)	118.2206
A(1,6,5)	119.7495		A(25,30,32)	127.1426		A(43,45,68)	120.8205
A(1,6,10)	120.5207		A(26,30,32)	122.7618		A(44,45,68)	120.9571
A(5,6,10)	119.7265		A(25,31,27)	109.7572		A(34,48,49)	110.8291
A(2,11,12)	122.7263		A(25,31,40)	128.5643		A(34,48,50)	111.9287
A(2,11,13)	117.0478		A(27,31,40)	121.4852		A(34,48,51)	110.3062
A(12,11,13)	119.342		A(30,32,33)	118.5499		A(49,48,50)	107.855
A(11,13,14)	118.2077		A(30,32,34)	118.9032		A(49,48,51)	107.564
A(11,13,23)	120.6134		A(33,32,34)	122.3624		A(50,48,51)	108.2038
A(14,13,23)	120.8686		A(32,33,35)	117.4908		A(33,52,53)	112.7744
A(13,14,16)	119.2622		A(32,33,52)	122.2483		A(33,52,54)	110.7116
A(13,14,17)	118.5243		A(35,33,52)	120.153		A(33,52,55)	110.3286
A(16,14,17)	122.1944		A(32,34,36)	117.3839		A(53,52,54)	107.1575
A(18,15,19)	121.6513		A(32,34,48)	122.2649		A(53,52,55)	107.9124
A(18,15,23)	120.9371		A(36,34,48)	120.2768		A(54,52,55)	107.7605
A(19,15,23)	117.3892		A(33,35,37)	122.0372		A(37,56,57)	111.4275
A(14,16,18)	118.9334		A(33,35,38)	118.5614		A(37,56,58)	110.7471
A(14,16,20)	120.3021		A(37,35,38)	119.3905		A(37,56,59)	111.4108
A(18,16,20)	120.754		A(34,36,37)	122.1506		A(57,56,58)	107.3545
A(15,18,16)	119.3822		A(34,36,39)	118.4871		A(57,56,59)	108.4515
A(15,18,21)	118.9513		A(37,36,39)	119.3565		A(58,56,59)	107.2637
A(16,18,21)	121.6631		A(35,37,36)	118.3073		A(41,60,61)	111.161
A(15,19,72)	154.2895		A(35,37,56)	120.8063		A(41,60,62)	110.0597
A(1,22,23)	85.3587		A(36,37,56)	120.8851		A(41,60,63)	112.2573
A(1,22,25)	94.715		A(31,40,41)	119.6905		A(61,60,62)	108.0263

Atom label	Angles
A(61,60,63)	107.0558
A(62,60,63)	108.1162
A(42,64,65)	110.4214
A(42,64,66)	110.422
A(42,64,67)	113.2352
A(65,64,66)	107.2731
A(65,64,67)	108.1261
A(66,64,67)	107.127
A(45,68,69)	110.7042
A(45,68,70)	111.3688
A(45,68,71)	111.4596
A(69,68,70)	107.2247
A(69,68,71)	107.4317
A(70,68,71)	108.4686

References

1. Bruker, *"APEX2" Bruker-AXS*. Madison, WI. USA, 2006.
2. Krause, L.; Herbst-Irmer, R.; Sheldrick, G. M.; Stalke, D., Comparison of silver and molybdenum microfocus X-ray sources for single-crystal structure determination. *J Appl Crystallogr* **2015,** *48* (Pt 1), 3-10.
3. Sheldrick, G. M., *SADABS, Program for bruker area detector absorption correction.* University of Gottingen, Gottingen, 1997.
4. Sheldrick, G. M., Crystal structure refinement with SHELXL. *Acta Crystallogr C Struct Chem* **2015,** *71* (Pt 1), 3-8.
5. Sheldrick, G. M., SHELXT - integrated space-group and crystal-structure determination. *Acta Crystallogr A Found Adv* **2015,** *71* (Pt 1), 3-8.
6. Parkin, S., Expansion of scalar validation criteria to three dimensions: the R tensor. Erratum. *Acta Crystallogr A* **2000,** *56* (Pt 3), 317.
7. Spek, A. L., Structure validation in chemical crystallography. *Acta Crystallogr D Biol Crystallogr* **2009,** *65* (Pt 2), 148-55.
8. Kim, J.; Hong, S. H., Ligand-Promoted Direct C–H Arylation of Simple Arenes: Evidence for a Cooperative Bimetallic Mechanism. *ACS Catalysis* **2017,** *7* (5), 3336-3343.
9. Hans, M.; Lorkowski, J.; Demonceau, A.; Delaude, L., Efficient synthetic protocols for the preparation of common N-heterocyclic carbene precursors. *Beilstein Journal of Organic Chemistry* **2015,** *11*, 2318-2325.
10. Herrmann, W. A.; Böhm, V. P. W.; Gstöttmayr, C. W. K.; Grosche, M.; Reisinger, C.-P.; Weskamp, T., Synthesis, structure and catalytic application of palladium(II) complexes bearing N-heterocyclic carbenes and phosphines. *Journal of Organometallic Chemistry* **2001,** *617–618*, 616-628.
11. Johnson, A.; Gimeno, M. C., An efficient and sustainable synthesis of NHC gold complexes. *Chemical Communications* **2016,** *52* (62), 9664-9667.
12. Block, B. P.; Bailar, J. C., The Reaction of Gold(III) with Some Bidentate Coördinating Groups1. *Journal of the American Chemical Society* **1951,** *73* (10), 4722-4725.
13. Kung, K. K., Lo, V. K., Ko, H. , Li, G. , Chan, P. , Leung, K. , Zhou, Z. , Wang, M. , Che, C. and Wong, M., Cyclometallated Gold(III) Complexes as Effective Catalysts for Synthesis of Propargylic Amines, Chiral Allenes and Isoxazoles. *Advanced Synthesis & Catalysis* **2013,** *355* (10), 2055-2070.
14. von Wachenfeldt, H.; Polukeev, A. V.; Loganathan, N.; Paulsen, F.; Röse, P.; Garreau, M.; Wendt, O. F.; Strand, D., Cyclometallated gold(iii) aryl-pyridine complexes as efficient catalysts for three-component synthesis of substituted oxazoles. *Dalton Transactions* **2015,** *44* (12), 5347-5353.